AMERICAN SOCIETY FOR MICROBIOLOGY | Molecular and Cellular Biology

The Zinc Finger of Prolyl Hydroxylase Domain Protein 2 Is Essential for Efficient Hydroxylation of Hypoxia-Inducible Factor α

Patrick R. Arsenault,[a] Daisheng Song,[a] Yu Jin Chung,[a]* Tejvir S. Khurana,[b] Frank S. Lee[a]

Department of Pathology and Laboratory Medicine, Perelman School of Medicine, University of Pennsylvania, Philadelphia, Pennsylvania, USA[a]; Department of Physiology and Pennsylvania Muscle Institute, Perelman School of Medicine, University of Pennsylvania, Philadelphia, Pennsylvania, USA[b]

Prolyl hydroxylase domain protein 2 (PHD2) (also known as EGLN1) is a key oxygen sensor in mammals that posttranslationally modifies hypoxia-inducible factor α (HIF-α) and targets it for degradation. In addition to its catalytic domain, PHD2 contains an evolutionarily conserved zinc finger domain, which we have previously proposed recruits PHD2 to the HSP90 pathway to promote HIF-α hydroxylation. Here, we provide evidence that this recruitment is critical both *in vitro* and *in vivo*. We show that *in vitro*, the zinc finger can function as an autonomous recruitment domain to facilitate interaction with HIF-α. *In vivo*, ablation of zinc finger function by a C36S/C42S *Egln1* knock-in mutation results in upregulation of the *erythropoietin* gene, erythrocytosis, and augmented hypoxic ventilatory response, all hallmarks of *Egln1* loss of function and HIF stabilization. Hence, the zinc finger ordinarily performs a critical positive regulatory function. Intriguingly, the function of this zinc finger is impaired in high-altitude-adapted Tibetans, suggesting that their adaptation to high altitude may, in part, be due to a loss-of-function *EGLN1* allele. Thus, these findings have important implications for understanding both the molecular mechanism of the hypoxic response and human adaptation to high altitude.

The hypoxia-inducible factor (HIF) pathway is the primary mediator of the transcriptional response to low oxygen (1–3). In this pathway, prolyl hydroxylase domain protein (PHD) site-specifically prolyl hydroxylates hypoxia-inducible factor α (HIF-α), thereby providing a recognition motif for the von Hippel-Lindau (VHL) protein, which then promotes the ubiquitination and degradation of HIF-α (4–6). Under hypoxic conditions, this modification is arrested, leading to the stabilization of HIF-α, its dimerization with HIF-β, and the subsequent activation of a transcriptional program that promotes hypoxic adaptation at the organismal and cellular levels (7, 8). There are two main HIF-α paralogues, HIF-1α and HIF-2α, which have overlapping and distinct roles. For example, HIF-1α promotes glycolysis, whereas HIF-2α (also known as EPAS1) regulates the *erythropoietin* (*EPO*) gene.

In mammals, there are three PHD paralogues (9, 10), and PHD2 has emerged as a particularly important one. For example, knockout of murine *Egln1* but not of *Egln2* (*Phd1*) or *Egln3* (*Phd2*) leads to embryonic lethality (11). In humans, heterozygous loss-of-function mutations in the *EGLN1* gene that impair catalytic activity are a cause of erythrocytosis (12). In mice, acute global deletion of *Egln1* leads to marked erythrocytosis (13, 14). Intriguingly, heterozygous loss of Phd2 function in mice leads to increased respiration (15, 16), and importantly, this phenotype is not observed in either $Egln2^{-/-}$ or $Egln3^{-/-}$ mice (15).

PHD2 is closely related to the single ancestral PHD that is present in simple metazoans, such as *Trichoplax adhaerens* (17). This orthologue shares, in addition to a C-terminal prolyl hydroxylase domain, an N-terminal zinc finger that is absent in both PHD1 and PHD3 (18). This zinc finger, which is of the myeloid nervy DEAF-1 (MYND) type, shows broad evolutionary conservation (17, 19). MYND-type zinc fingers in other proteins typically serve as domains that interact with other proteins (20). For example, the MYND-type zinc finger of the transcriptional regulator ETO binds to a Pro-Pro-Pro-Leu-Ile motif in the corepressor SMRT (21).

We have recently shown that the zinc finger of PHD2 binds with high stringency to a Pro-Xaa-Leu-Glu motif that is found in select proteins of the HSP90 pathway, including p23, FKBP38, and HSP90 itself (22, 23). This leads to a model in which the zinc finger promotes recruitment of PHD2 to the HSP90 pathway to facilitate hydroxylation of HIF-α, a known HSP90 client protein. In order to test this model, here, we first employed an *in vitro* system to demonstrate that the zinc finger fused to a heterologous protein can, in a manner independent of the catalytic domain, promote recruitment to HIF-α. To assess the role of the zinc finger of PHD2 *in vivo*, we generated a knock-in mouse model in which we ablated the zinc finger. We found that these mice displayed erythrocytosis and increased respiration, both indicative of Hif pathway activation and loss of Phd2 function. Taken together, these findings support a model in which the zinc finger has a positive regulatory function. Strikingly, Tibetans harbor a PHD2 variant that is defective in its interaction with p23, a key cochaperone for HSP90 (23). Hence, these studies support the notion that Tibetan *EGLN1* is likely to be a loss-of-function allele that promotes adaptation to chronic hypoxia.

Received 10 February 2016 **Returned for modification** 9 March 2016
Accepted 12 June 2016

Accepted manuscript posted online 20 June 2016

Citation Arsenault PR, Song D, Chung YJ, Khurana TS, Lee FS. 2016. The zinc finger of prolyl hydroxylase domain protein 2 is essential for efficient hydroxylation of hypoxia-inducible factor α. Mol Cell Biol 36:2328–2343. doi:10.1128/MCB.00090-16.

Address correspondence to Frank S. Lee, franklee@mail.med.upenn.edu.

* Present address: Yu Jin Chung, Department of Physiology, Anatomy, and Genetics, University of Oxford, Oxford, United Kingdom.

Supplemental material for this article may be found at http://dx.doi.org/10.1128/MCB.00090-16.

MATERIALS AND METHODS

Plasmids. Plasmids were constructed by standard methods. Details of cloning and subcloning, including oligonucleotide sequences, can be found in the supplemental material. The authenticity of all constructs was confirmed by Sanger sequencing.

Peptide binding assays. Peptides corresponding to p23 (151–160) or p23 (151–160) P157A/L159A/E160A, FKBP38 (47–56), HSP90α (711–720), and HSP90β (703–712) have been described previously (22, 23). The peptides (0.5 μg) were prebound to 15-μl aliquots of streptavidin-agarose (Sigma). The resins were incubated with lysates from HEK293FT cells previously transfected using Lipofectamine 2000 with constructs for EGFP-PHD2 (1–63) or mutants thereof. Lysates were prepared in buffer A (20 mM Tris, pH 7.6, 150 mM NaCl, 10% glycerol, 1% Triton X-100) supplemented with 1 μM $ZnCl_2$ and mammalian cell protease inhibitor cocktail (Sigma). Incubations were performed for 2 h with rocking at 4°C. The resins were washed four times with buffer A supplemented with 1 μM $ZnCl_2$ and eluted, and the eluates were subjected to SDS-PAGE and Western blotting using rabbit anti-green fluorescent protein (anti-GFP) antibody (FL; Santa Cruz Biotechnology), followed by anti-rabbit IgG conjugated to alkaline phosphatase.

***In vitro* biotinylation assays.** Proteins were prepared by TNT T7 Quick coupled transcription/translation reticulocyte lysate reactions (Promega). In a typical reaction, 0.2 μg of plasmid template was incubated with TNT T7 Quick master mix, 50 μM methionine, 1 μM zinc, and 10 μM biotin in a total volume of 10 μl at 30°C for 60 min. BirA or BirA fusion protein, obtained in separate TNT T7 Quick coupled transcription/translation reactions, was included, as appropriate. The products were subjected to SDS-PAGE, transferred to Immobilon-P membranes (EMD Millipore), and blocked in Tris-buffered saline–5% nonfat milk. Far-Western blotting was performed using streptavidin coupled to alkaline phosphatase (USB 11687). CDP-Star (Roche) was employed as a substrate.

Cell culture and transfections. HEK293FT cells were maintained, transfected, and harvested for Western blotting as described previously (22). Hypoxia experiments were performed in an In Vivo 200 Hypoxia Work Station (Ruskinn Technologies). MG132 was obtained from Sigma.

Gene targeting. The construct for generating the *Egln1* allele bearing a C36S/C42S mutation (*Egln1*^{ZF}) was prepared by recombineering (24). In brief, a mini-targeting vector was constructed in the vector pL452 (25). The mini-targeting vector contained genomic DNA encompassing exon 1 of the mouse *Egln1* gene with nucleotide changes encoding the C36S/C42S mutation. A silent, diagnostic XhoI site was also introduced in the vicinity of the C36S/C42S mutation. The vector contained a neomycin selection cassette flanked by *loxP* sites and additional sequences downstream of exon 1. A retrieval plasmid was constructed in the vector pMC1-DTA (26). This retrieval plasmid contained sequences that flank 12 kb of genomic-DNA sequence at the mouse *Egln1* locus, as well as a diphtheria toxin A negative-selection cassette. This retrieval plasmid was used to capture, by recombineering, 12 kb of mouse *Egln1* genomic DNA containing exon 1 from C57BL/6 bacterial artificial chromosome (BAC) clone RP23-356I16 (Invitrogen). The resulting product was then used, in the second recombineering step with the mini-targeting vector, to generate the final targeting vector. This targeting vector has an 8.3-kb 5′ arm containing the murine *Egln1* exon 1 with the C36S/C42S knock-in mutation, a neomycin selection cassette flanked by *loxP* sites, and a 3.7-kb 3′ arm (see Fig. 4A). The presence of the desired nucleotide changes and the integrity of exon 1 were confirmed by DNA sequencing.

V6.5 embryonic stem (ES) cells were electroporated with the targeting vector and selected, using G418, by the Perelman School of Medicine Gene Targeting Core Facility. Screening was performed by Southern blotting. Digoxigenin (DIG)-labeled probes were generated by PCR using a PCR DIG probe synthesis kit (Roche). For the 5′ probe (0.40 kb), the primers were 5′-TTA TCA TTA TCA ATT GGT TCT G-3′ and 5′-TGT TCT CTG AAC CCC TCG TGT GCC-3′. For the 3′ probe (0.40 kb), the primers were 5′-TCT CTG TGC TGC GGT TAA TTA GTC-3′ and 5′-

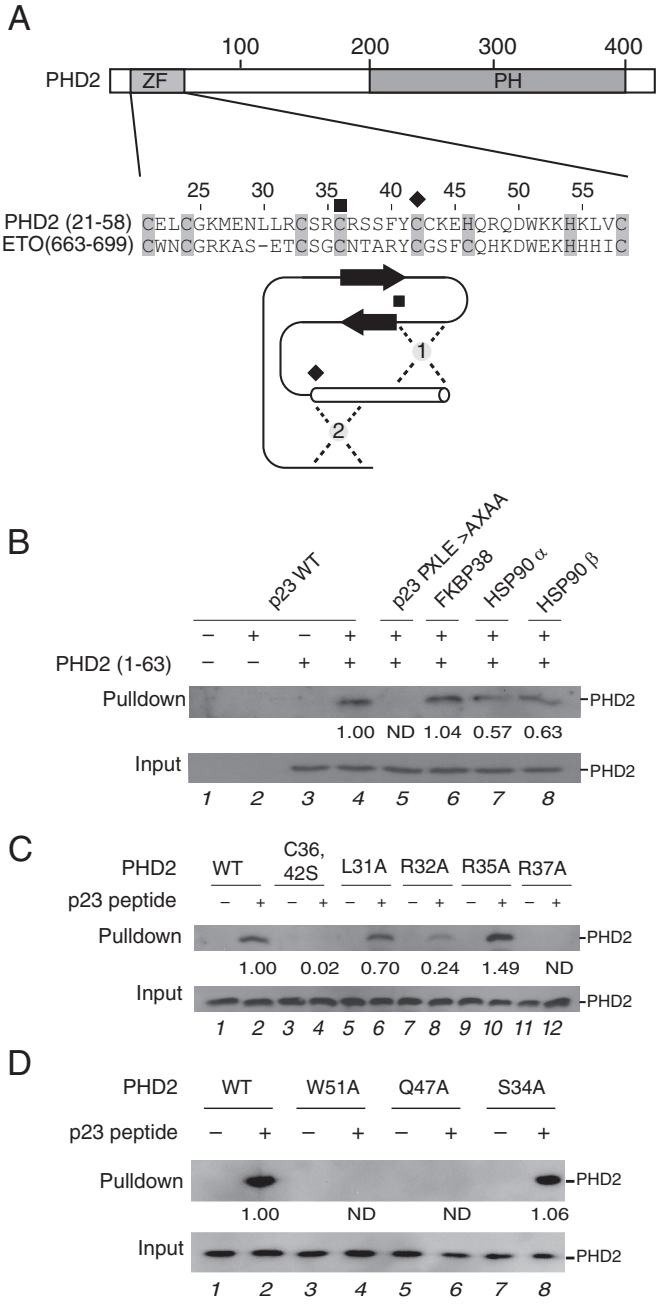

FIG 1 The N terminus of PHD2 has a MYND-type zinc finger motif, and mutagenesis identified key residues. (A) (Top) Location of the predicted zinc finger (ZF) in PHD2. PH, prolyl hydroxylase domain. The numbers are amino acids. (Middle) Comparison between the zinc fingers of PHD2 and ETO. The numbers are PHD2 residue numbers, and the shaded boxes represent zinc-chelating residues. ■ and ◆ denote C36 and C42 of PHD2, respectively. (Bottom) Predicted topology of the MYND zinc finger of PHD2, based on the X-ray crystal structure of the homologous MYND zinc finger from the ETO protein (21). 1 and 2 indicate zinc ions. The arrows and cylinder represent β-pleated sheets and α-helix, respectively. (B) WT PHD2 (1–63) fused to GFP and expressed in HEK293FT cells was incubated with or without immobilized p23 (151–160), FKBP38 (47–56), HSP90α (711–720), HSP90β (703–712), or mutant p23 (151–160) peptide; washed; and eluted. GFP-PHD2 (1–63) was detected by Western blotting using anti-GFP antibodies. (C and D) WT or mutant PHD2 (1–63) fused to GFP and expressed in HEK293FT cells was incubated with or without immobilized p23 (151–160), washed, and eluted. PHD2 was detected as for panel B. The numbers below the bands indicate relative intensities by densitometry compared to WT p23 (B) or WT PHD2 (C and D). ND, not detectable.

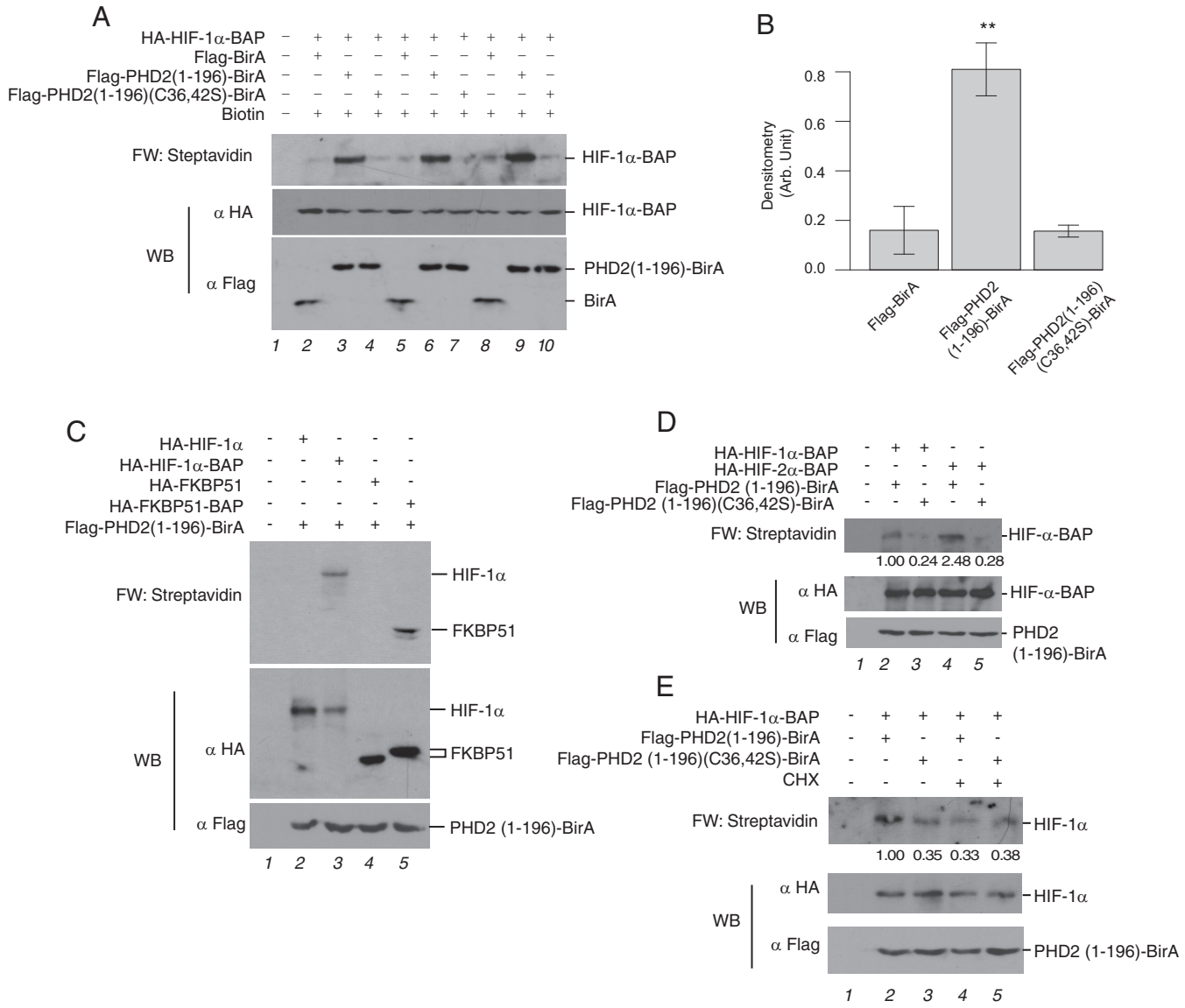

FIG 2 The zinc finger of PHD2 can function autonomously *in vitro* to promote recruitment to HIF-α. (A and C to E) *In vitro* transcription and translation reactions were performed with constructs for the indicated proteins in the absence or presence of previously translated BirA or BirA fusion proteins, as indicated. The reactions were analyzed by far-Western (FW) blotting using streptavidin-alkaline phosphatase conjugates and Western blotting (WB) using the indicated antibodies. The numbers below the bands indicate the results of densitometry analysis normalized to WB of BAP-containing protein. (A) Biotinylation of HA-tagged HIF-1α containing a BAP motif is enhanced by fusion of BirA to PHD2 (1–196) relative to fusion to PHD2 (1–196) (C36,42S) or BirA alone. (B) Densitometry analysis was performed on biotinylation signals and normalized for loading to the anti-HA WB densitometry signal. The graph shows the mean densitometry across the three replicates, and the errors bars are standard errors of the mean (SEM). **, $P < 0.01$ by ANOVA/Tukey HSD. Arb., arbitrary. (C) PHD2 (1–196)-BirA can efficiently biotinylate BAP-containing HIF-1α and FKBP51 proteins, and biotinylation is dependent on the BAP motif. (D) WT PHD2 (1–196)-BirA can promote biotinylation of both HIF-1α–BAP and HIF-2α–BAP in a manner dependent on zinc finger integrity. (E) Zinc finger dependence of PHD2 (1–196)-BirA-induced biotinylation of HIF-1α–BAP is attenuated when the former is added after HIF-1α–BAP translation is completed and then arrested by the addition of cycloheximide (CHX). *In vitro* transcription and translation reactions were performed for HIF-1α–BAP. In lanes 2 and 3, previously translated BirA fusion protein was included in the 60-min reaction. In lanes 4 and 5, HIF-1α–BAP was first translated, CHX (2 μg/ml) was added for 30 min, and then the previously translated BirA fusion protein was added for an additional 60 min.

ACA TTA TGA CTC CTA ACA ATA GCG-3′. For both probes, BAC clone BAC RP23-356I16 was employed as the template. Southern blotting was performed using DIG Easy Hyb, a DIG wash-and-block buffer set, antidigoxigenin-alkaline phosphatase conjugates, and CDP-Star substrate (all from Roche).

A total of 192 clones were screened by Southern blotting. Southern blotting of a correctly targeted clone with a 5′ probe revealed the expected 16.3 kb for the *Egln1*^{ZF} allele upon hybridization with HindIII-digested DNA, in addition to the wild-type (WT) 8.9-kb band (see Fig. 4B, lane 2). Southern blotting with a 3′ probe revealed the expected 16.3-kb band for the *Egln1*^{ZF} allele upon hybridization with HindIII-digested DNA, in addition to the wild-type 5.4-kb band (see Fig. 4B, lane 7). Sequencing confirmed the presence of the desired sequence for the *Egln1*^{ZF} allele (see Fig. 4C).

The correctly targeted clone was injected into BALB/c blastocysts to produce chimeras by the Perelman School of Medicine Transgenic Core

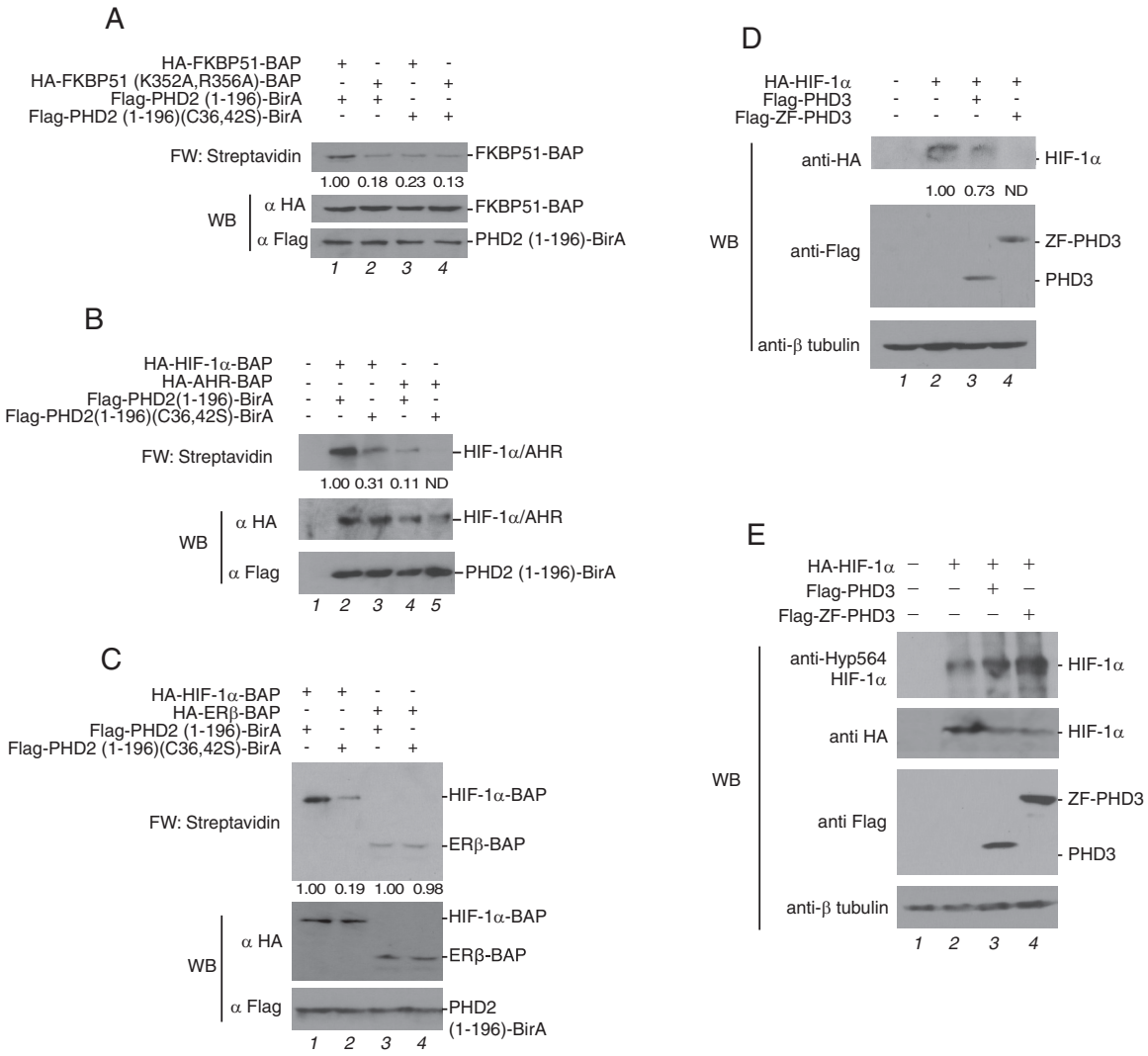

FIG 3 The zinc finger of PHD2 shows specificity for HIF-α over other HSP90 client proteins and can enhance PHD3 activity. (A) Biotinylation of FKBP51-BAP by PHD2 (1–196)-BirA is dependent on the integrity of the FKBP51-HSP90 interaction and the PHD2 zinc finger. (B) Biotinylation of AHR by PHD2 is significantly reduced relative to HIF-1α and is dependent on the integrity of the PHD2 zinc finger. (C) PHD2-BirA fusion proteins do not efficiently biotinylate the HSP90 client protein ERβ fused to BAP. (D) Western blot analysis of HEK293FT cells transfected with HA–HIF-1α vector and either vector control, Flag-PHD3, or Flag-ZF-PHD3, followed by 4 h of hypoxia (2% O_2), showing decreased HIF-1α abundance with coexpressed ZF-PHD3 fusion relative to coexpressed PHD3. The numbers below the bands indicate the results of densitometry analysis normalized to β-tubulin. ND, not detectable. (E) HEK293FT cells were cotransfected with an expression vector for HA–HIF-1α with or without a vector for PHD3, zinc finger PHD3 fusion protein, or vector control and treated with 10 μM MG132 for 4 h. The lysates were probed for hydroxylated HIF-1α (Hyp564), total HA–HIF-1α, Flag-PHD3, and β-tubulin.

Facility, which is supported by the Institute for Diabetes, Obesity, and Cardiovascular Metabolism; the Center for Molecular Studies in Digestive and Liver Diseases; and the Abramson Cancer Center. Chimeric male mice were then mated with C57BL/6J-*Tyr*$^{c\text{-}2J}$ female mice, and germ line transmission (as assessed by coat color and then PCR) was obtained. Southern blotting confirmed germ line transmission (see Fig. 4B, lanes 4 and 9). Mice with germ line transmission of the knock-in allele were then mated with C57BL/6-Gt(*ROSA*)*26Sor*$^{tm16(Cre)Arte}$ mice (Taconic) to delete the neomycin cassette (see Fig. 4B, lanes 5 and 10), followed by further crossing with C57BL/6 mice to segregate the Cre allele, thereby creating *Egln1*$^{ZF/+}$ mice. *Egln1*$^{ZF/+}$ mice were maintained on a mixed 129/C57BL/6 background. *Egln1*$^{ZF/ZF}$ mice were obtained by *Egln1*$^{ZF/+}$ intercrosses.

The *Egln1*$^{+/-}$, *Egln1*$^{f/f}$, and Pax3-Cre lines have all been described previously (16). All animal procedures were approved by the Institutional Animal Care and Use Committees at the University of Pennsylvania, in compliance with Animal Welfare Assurance.

PCR genotyping. DNA was isolated from mouse tails (27). The following primers were employed for genotyping the *Egln1* C36S/C42S knock-in mutation. CSint1-1 5′, 5′-CCA GAC ACT GTG TTT AGC TAG GAC-3′, and CSint1-1 3′, 5′-AAA CCA GGA AGC CAC AGA AGC AGC-3′. The wild-type allele produces a PCR product of 0.30 kb, whereas the knock-in mutant allele produces a PCR product of 0.40 kb.

Hematology analyses. Retro-orbital blood samples for hematology analyses were collected in Microvette 100 LH heparin-coated collection tubes (Sarstedt). Hematocrit (HCT) was measured manually using a CritSpin microhematocrit centrifuge (StatSpin). Automated CBC analysis was performed using a Hemavet 950FS instrument (Erba Diagnostics).

Serum Epo and iron measurements. Serum samples were obtained by incubating terminal bleeds from the inferior vena cava at 4°C, followed by

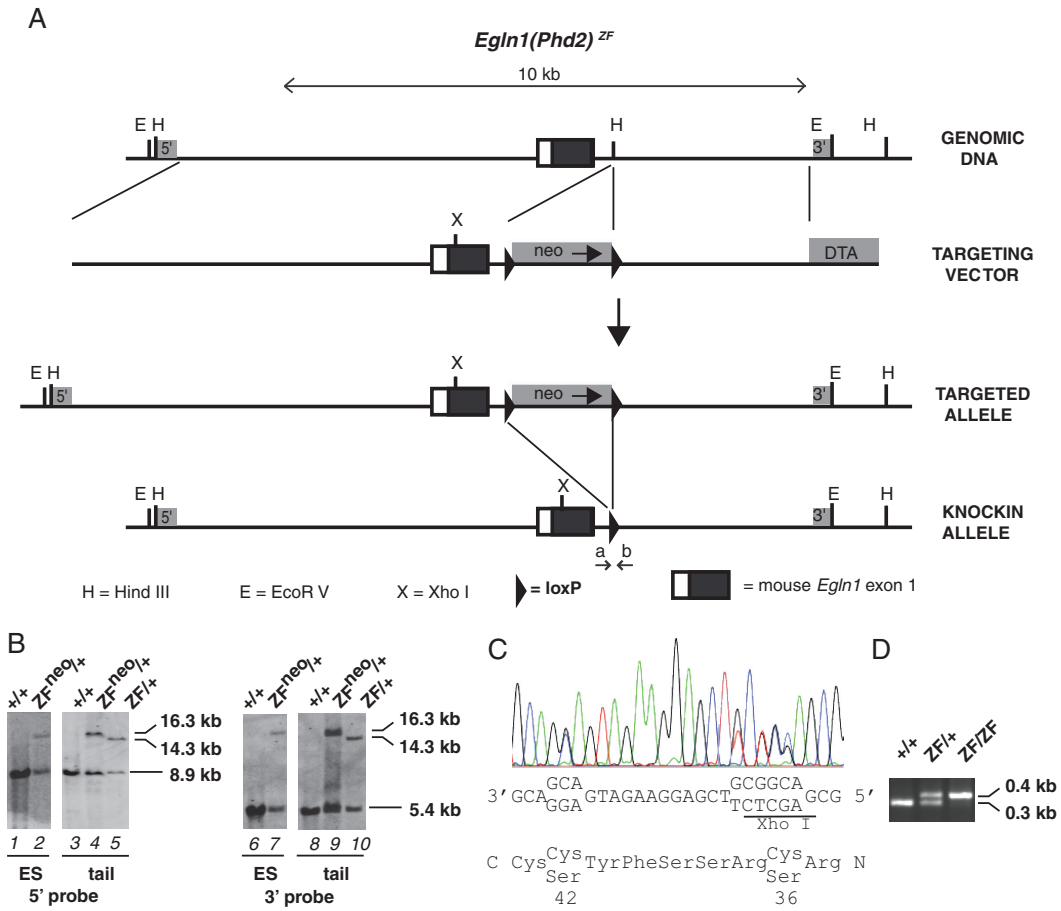

FIG 4 Generation of *Egln1*^{ZF} knock-in mice. (A) Gene-targeting strategy. X indicates both the site of mutation and the diagnostic XhoI site. DTA, diphtheria toxin A; neo, neomycin cassette. The positions of 5′ and 3′ Southern probes are indicated by 5′ and 3′, respectively. The positions of CSint1-1 5′ and CSint1-1 3′ PCR primers are indicated by a and b, respectively. (B) Southern blots employing 5′ (left) and 3′ (right) probes of HindIII-digested ES cell or mouse tail DNA. *Egln1* genotypes are provided at the top. The presence of the neomycin cassette is denoted by neo. (C) DNA-sequencing chromatogram of targeted ES cell DNA. The sequence is from 3′ to 5′ (reverse complement). The codons at residues 36 and 42 are each heterozygous for Cys and Ser. (D) PCR genotyping of *Egln1*^{ZF} knock-in mice using CSint1-1 5′ and CSint1-1 3′ primers. The 0.3-kb product is derived from the wild-type allele, while the 0.4-kb product is derived from the ZF mutant allele. *Egln1* genotypes are shown at the top.

centrifugation at 4,000 × *g* for 15 min at 4°C. Serum Epo measurements were performed using the rodent Quantikine Epo Immunoassay kit (R&D Systems; MEP00B). Serum iron measurements were performed using the Iron-SL kit (Sekisui Diagnostics). Plate absorbances were read on a Sunrise microplate reader (Tecan).

Real-time PCR. RNA was isolated from approximately 125-mm^3 sections of either liver, kidney, heart, or placenta, as indicated; alternatively, approximately 50 μl of enterocytes from duodenal scrapings was employed as source material. In addition, primary duodenal epithelial cell cultures were used as source material and established following a procedure described previously (28). Briefly, duodenums were excised from 4-month-old *Egln1*$^{+/+}$ and *Egln1*$^{ZF/ZF}$ mice, and epithelial cells were dissociated using cell recovery solution (Corning) and mild agitation. The isolated epithelial cells were plated and maintained in Dulbecco's modified Eagle's medium (DMEM) with 5% fetal bovine serum (FBS), 4.5 g/liter glucose, 4 mM glutamine, 5 ng/ml epidermal growth factor, 0.2 IU/ml insulin, 20 mM HEPES, 100 U/ml penicillin, and 100 μg/ml streptomycin. The cells were maintained for 2 days under a normoxic (21% O_2 and 5% CO_2) or hypoxic (4% O_2 and 5% CO_2) environment prior to RNA isolation for real-time PCR. The details of RNA isolation, cDNA synthesis, and real-time PCR cycling conditions have been described previously (16).

Primer sequences for *Epo*, *Egln3*, *Vegfa*, and *Pgk1* have also been described previously (29). For *Cybrd1* (*Dcytb*), the following primers were used: SG-mDcytB 5′, GCA GCG GGC TCG AGT TTA, and SG-mDcytB 3′, TTC CAG GTC CAT GGC AGT CT. For *Hamp1* (*Hepc*), the following primers were used: SG-mHEPC 5′, TGT CTC CTG CTT CTC CTC CT, and SG-mHEPC 3′, CTC TGT AGT CTC TCT CAT CTG TTG. For *Slc11a2* (*Dmt1*), the following primers were used: SG-mDMT1 5′, GTC TCT GGC GCT GCC ATT, and SG-mDMT1 3′, GCT CCT GAG ATT GCC TTC TGA. For *Tfeb*, the following primers were used: SG-mTFEB 5′, GGA CGT GCG CTG GAA CA, and SG-mTFEB 3′, CCT CCG GAT GTA ATC CAC AGA. For *Gcm1*, the following primers were used: SG-mGCM1 5′, CGA CGG ACG CTT CAT CTT TT, and SG-mGCM1 3′, GGC CTG GGA TGA TCA TGC T. For *Ascl2* (*Mash2*), the following primers were used: SG-mMASH2 5′, CCT GGG CCT ATG CCT TAC C, and SG-mMASH2 3′, TCA GTC AGC ACT TGG CAT TTG. For *Slc2a1* (*Glut1*), the following primers were used: SG-mGlut1 5′, CGA GGG ACA GCC GAT GTG, and SG-mGlut1 3′, TGC CGA CCC TCT TCT TTC AT. For *Angpt2*, the following primers were used: SG-mAngpt2 5′, GAT GGC AGT GTG GAC TTC CA, and SG-mAngpt2 3′, GCT CCC GAA GCC CTC TTT.

Western blotting. Protein extracts were prepared from kidney, liver, and heart tissue by solubilization (with sonication) in T-PER

TABLE 1 Genotypes and embryonic viability assessments for *Egln1*$^{ZF/+}$ × *Egln1*$^{ZF/+}$ matings

Day	No. of embryos (no. viable)		
	Egln1$^{+/+}$	*Egln1*$^{ZF/+}$	*Egln1*$^{ZF/ZF}$
E11.5	8 (8)	15 (15)	7 (7)
E12.5	8 (8)	11 (11)	6 (4)
Total	16	36	13

tissue protein extraction reagent (Thermo Scientific) supplemented with mammalian protease inhibitor cocktail (Sigma P8340). Insoluble material was removed by centrifugation at 8,600 × *g* for 10 min at 4°C. Western blotting was performed on equal protein amounts, as determined by DC protein assay (Bio-Rad). Anti-PHD2 rabbit monoclonal antibody (MAb) (D31E11), anti-hydroxy-Pro564-HIF-1α (Hyp564-HIF-1α) rabbit MAb (D43B5), anti-HIF-1α rabbit MAb (D2U3T), and anti-β-tubulin rabbit MAb (9F3; used for Western blots of mouse tissue extracts) were obtained from Cell Signaling Technology. Anti-HIF-2α rabbit MAb (ab179825) was from Abcam. Anti-β-tubulin mouse MAb (E7; used for Western blots of HEK293FT extracts) was generated by Michael Klymkowsky and was obtained from the Developmental Studies Hybridoma Bank developed under the auspices of the NICHD and maintained by the Department of Biology, University of Iowa, Iowa City, IA. Rabbit polyclonal antibodies to GFP (FL; sc-8334) and α-tubulin (H-300; sc-5546), goat anti-rabbit IgG secondary antibodies conjugated to alkaline phosphatase (sc-2007), and goat anti-mouse IgG secondary antibodies conjugated to alkaline phosphatase (sc-2008) were obtained from Santa Cruz Biotechnology. Antihemagglutinin (anti-HA) and anti-Flag antibodies coupled to alkaline phosphatase were from Sigma (A5477 and A9649, respectively). Band densitometry was performed on scanned immunoblots using the ImageJ gel analysis software (30).

BFU-E assay. Burst-forming unit–erythroid (BFU-E) assays were performed as previously described, and final counts were performed after 9 days of culture (16).

Pulmonary function measurements. Lung function was assessed by whole-body plethysmography as previously described (16). Tidal volumes were calculated from integrating raw Powerlab pneumotachometer data based on the methods described previously (31) for whole-body plethysmography chambers. Tidal volume (V_t) and minute ventilation (V_e) were further normalized to body mass.

Structural modeling. A model for the zinc finger of PHD2 bound to a p23 peptide was generated as follows. First, a structure of PHD2 (20–59) was generated with SWISS-MODEL using the X-ray crystal structure of the MYND zinc finger of ETO bound to a SMRT peptide (Protein Data Bank [PDB] 2ODD) as a basis (21). The resulting PHD2 (20–59) structure was next superimposed on the structure of the ETO:SMRT peptide complex using the Chimera software package (UCSF) (32). Amino acids 1101 to 1109 of SMRT were replaced by amino acids 152 to 160 of p23, and the ETO structure was then deleted to produce a preliminary PHD2 (20–59):p23 (152–160) structure model. Peptide binding was then further refined using Rosetta FlexPepDock (33).

Statistical analyses. Real-time PCR (ΔC_T), lung function parameters, EPO enzyme-linked immunosorbent assay (ELISA), and serum iron were assessed for statistical significance by Student *t* tests. Hematologic measurements in which *Egln1*$^{ZF/+}$ heterozygous mice were included were analyzed by analysis of variance (ANOVA) and *post hoc* Tukey honestly

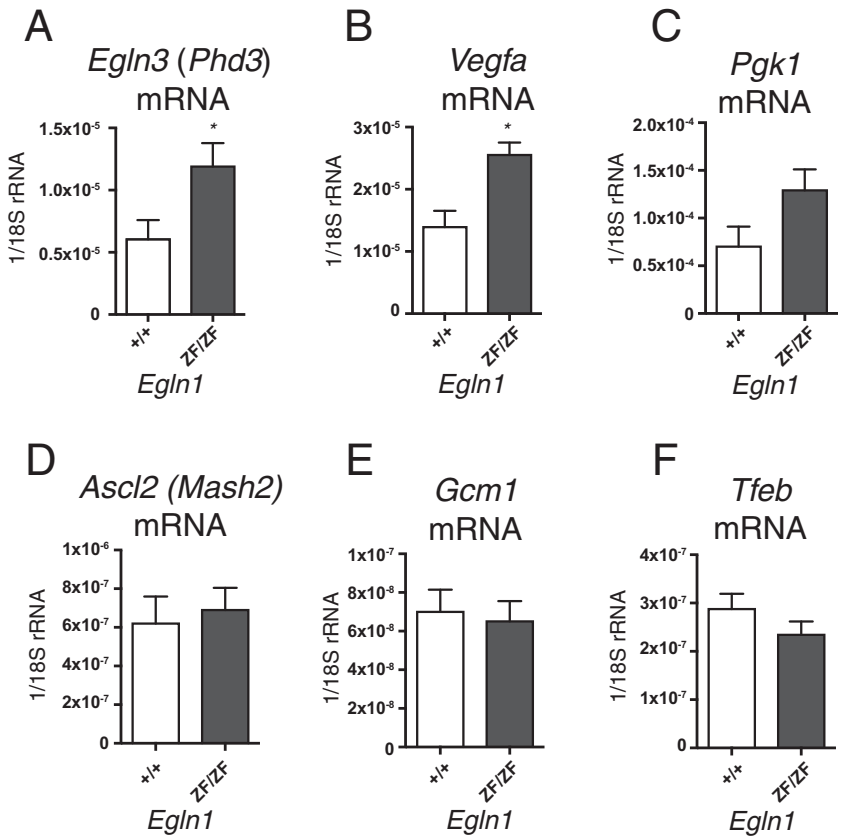

FIG 5 (A to F) Real-time PCR mRNA analysis of E11.5 placental tissue from *Egln1*$^{+/+}$ and *Egln1*$^{ZF/ZF}$ embryos ($n = 4$). *, $P < 0.05$ by Student's *t* test. The error bars represent SEM.

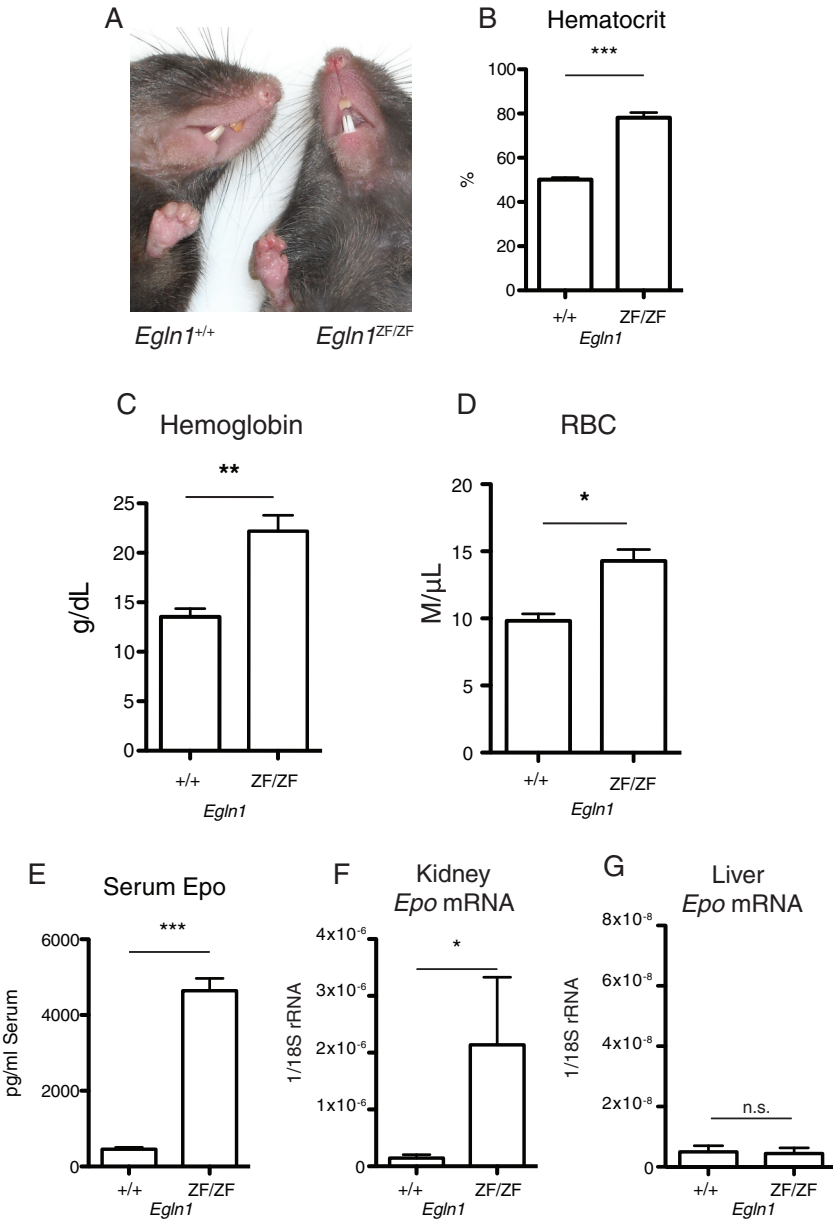

FIG 6 *Egln1*$^{ZF/ZF}$ mice display elevations of Epo and erythrocytosis. (A) *Egln1*$^{ZF/ZF}$ mice (right) appear plethoric compared to *Egln1*$^{+/+}$ controls (left). (B to E) Six-month-old *Egln1*$^{ZF/ZF}$ mice show increased hematocrit (B), hemoglobin (C), red blood cell counts (D), and serum Epo (E). The error bars represent SEM. $n = 5$ per group. *, $P < 0.05$; **, $P < 0.01$; ***, $P < 0.001$ by Student's *t* test. (F and G) Real-time PCR analysis of renal (F) and hepatic (G) *Epo* mRNA levels (relative to 18S rRNA). The error bars represent SEM. $n = 5$ per group. *, $P < 0.05$ by Student's *t* test; n.s., not significant.

significant difference (HSD) tests. The BFU-E results were analyzed by Poisson exact test. Statistical calculations were performed using the R software environment for statistical computing (R Foundation for Statistical Computing, 2010 [http://www.R-project.org]). A *P* value of <0.05 was used as a critical value for statistical significance.

RESULTS

Interaction of the PHD2 zinc finger with the PXLE motif is dependent on zinc finger integrity. The predicted MYND-type zinc finger of PHD2 is a member of a distinctive subclass of zinc fingers that has a cross brace topology, binds to two zinc ions, and has eight zinc-chelating residues (Fig. 1A). To examine the roles of individual amino acids in the zinc finger of PHD2, we incubated PHD2 (1–63) (fused to GFP) with immobilized, biotinylated p23 (151–160) peptide and assessed binding of the former by Western blotting. As expected, a mutation of the PXLE motif in the p23 peptide to AXAA abolished the interaction (Fig. 1B, lane 5), as did a C36S/C42S mutation in PHD2, which changes two predicted zinc-chelating residues (Fig. 1C, lane 4). Also as expected, WT PHD2 (1–63) can bind to PXLE-containing peptides derived from FKBP38, HSP90α, and HSP90β (Fig. 1B, lanes 6 to 8), which were previously identified in PHD2 immunoprecipitation experiments (22, 23).

The zinc finger of ETO is homologous to that of PHD2 (Fig. 1A), and previous studies identified critical roles for Gln-688 and

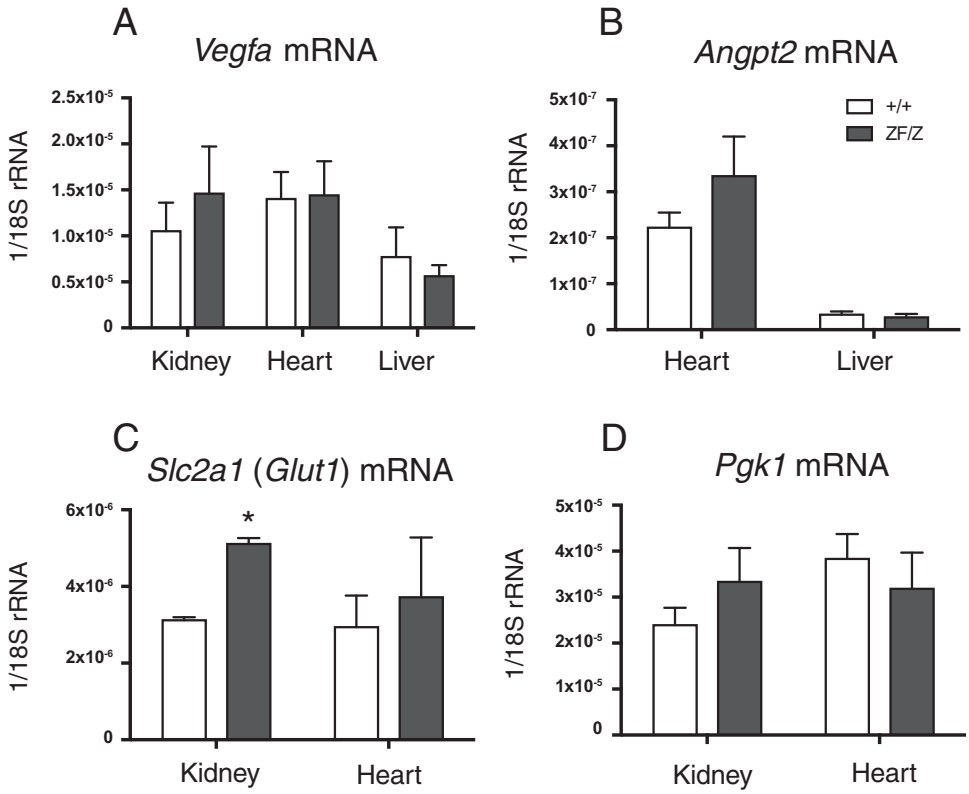

FIG 7 Real-time PCR mRNA analysis of Hif target genes from *Egln1*$^{+/+}$ and *Egln1*$^{ZF/ZF}$ mouse tissues at 2 months ($n = 4$). *, $P < 0.05$ by Student's *t* test. The error bars represent SEM.

Trp-692 in ETO binding to the Pro-Pro-Pro-Leu-Ile motif in SMRT (21). Mutation of the corresponding residues in PHD2, Gln-47 and Trp-51, respectively, abrogates binding to the p23 peptide (Fig. 1D, lanes 4 and 6). Homology modeling based on the known structure of ETO suggests that PHD2 Leu-31, Arg-32, Ser-34, Arg-35, and Arg-37 may be surface-exposed residues in the vicinity of these two residues. We found that while the L31A, S34A, and R35A mutations largely maintained the interaction, the R32A and R37A mutations markedly diminished it (Fig. 1C and D). Taken together, these studies support the notion that the PHD2 zinc finger is a MYND-type zinc finger.

The PHD2 zinc finger can function as an autonomous recruitment domain. In contrast to the C-terminal catalytic domain, the N-terminal zinc finger of PHD2 does not interact directly with HIF-α. Instead, we have proposed that the zinc finger recruits PHD2 to the HSP90 pathway to facilitate hydroxylation of HIF-α (22). To test whether the zinc finger of PHD2 can act autonomously in its association with the HSP90 pathway, we sought to uncouple the zinc finger domain from the prolyl hydroxylase domain. To this end, we fused PHD2 (1–196), which lacks the catalytic domain, to the *Escherichia coli* biotin ligase, BirA. We added this protein prior to initiation of *in vitro* transcription/translation reactions employing a template that encodes a HIF-1α construct in which the primary hydroxyl acceptor proline of the oxygen-dependent degradation domain had been replaced by a biotin acceptor peptide (BAP). In so doing, we allowed the fusion protein to act on HIF-α as it was folded by the HSP90 pathway. We examined biotinylation of the BAP-containing proteins by far-Western blotting using a streptavidin-alkaline phosphatase probe.

In a control reaction, we found that BirA alone can weakly biotinylate HIF-1α–BAP (Fig. 2A, lane 2) and that biotinylation is dependent on the presence of biotin (data not shown). Importantly, biotinylation is markedly enhanced by fusion of BirA to PHD2 (1–196) (lane 3). This enhancement is dependent on the presence of an intact zinc finger, as the C36S/C42S PHD2 mutant showed reduced biotinylation levels (lane 4) relative to WT PHD2 (1–196). Densitometry analysis of replicate *in vitro* translation and biotinylation reactions indicated this result is reproducible and statistically significant (Fig. 2A and B). Biotinylation is, as expected, dependent on the embedded BAP sequence, since wild-type HIF-1α is not biotinylated (Fig. 2C, lanes 2 and 3).

The C36S/C42S zinc finger mutation reduces the capacity of PHD2 (1–196)-BirA to biotinylate both HIF-1α–BAP and HIF-2α–BAP proteins (Fig. 2D). We observed somewhat stronger biotinylation of HIF-2α–BAP than of HIF-1α–BAP in these *in vitro* experiments. However, further experiments will be needed to establish if the zinc finger of PHD2 has an *in vivo* preference for one or the other isoform. In these experiments, the PHD2 (1–196)-BirA fusion protein was present during HIF-α translation, allowing the fusion protein to act while the HSP90 pathway promoted folding of the substrate. Consistent with this notion, if the PHD2 zinc finger-BirA fusion protein was added after the *in vitro* translation reaction was performed and then arrested by the addition of cycloheximide, the zinc finger enhancement of biotinylation was attenuated (Fig. 2E, lanes 4 and 5).

These data suggest that the fusion protein might be able to biotinylate other proteins of the HSP90 pathway. FKBP51 is an HSP90 cochaperone that immunoprecipitates with PHD2 (22)

and lacks a PXLE motif. When it is fused to BAP, it can be biotinylated by PHD2 (1–196)-BirA in a manner dependent on both the BAP sequence and the integrity of the PHD2 zinc finger (Fig. 2C, lanes 4 and 5, and 3A, lanes 1 and 3). Moreover, this effect is dependent on FKBP51 association with the HSP90 complex, since biotinylation is attenuated by an FKBP51 mutation (K352A and R356A) (34) that impairs its interaction with HSP90 (Fig. 3A, lane 2).

To determine if PHD2 is simply recruited equally to all HSP90-associated complexes, we examined biotinylation of a different HSP90 client protein and alternate transcription factor binding partner to HIF-β, the aryl hydrocarbon receptor (AHR). An AHR-BAP fusion protein was *in vitro* translated in the presence of either WT PHD2 (1–196)-BirA or PHD2 (1–196) (C36S and C42S)-BirA. At roughly comparable protein expression levels, HIF-1α-BAP was much more efficiently biotinylated than AHR-BAP, suggesting a selectivity for HSP90 complexes associated with HIF-1α (Fig. 3B, lanes 2 and 4). Furthermore, biotinylation of AHR-BAP was decreased to undetectable levels by mutation of the PHD2 zinc finger (lane 5). The latter result further supports our hypothesis that the zinc finger mediates association with the HSP90 complex and that its integrity is critical to this association.

Another alternative HSP90 client protein, albeit less well characterized in this regard than AHR, is estrogen receptor β (ERβ), and it was also used as a control for specificity. Compared to HIF-1α–BAP, an ERβ-BAP fusion was less efficiently biotinylated and, furthermore, showed no dependence on zinc finger integrity (Fig. 3C). Together with the data on HIF-1α and AHR, this supports a model in which the zinc finger of PHD2 recruits it to select HSP90 complexes, particularly ones involved in the folding of HIF-α proteins.

In an independent approach, we examined whether addition of the PHD2 zinc finger to the N terminus of PHD3 (which lacks a zinc finger) can augment PHD3 activity. To this end, we cotransfected HEK293FT cells with expression vectors for HIF-1α and for either PHD3 or a fusion protein containing the PHD2 zinc finger fused to the N terminus of PHD3 (ZF-PHD3). We exposed cells to hypoxia (2% O_2) for 4 h to stabilize HIF-1α and then examined protein levels by Western blotting. As shown in Fig. 3D, coexpression of PHD3 decreases HIF-1α protein levels (lanes 2 and 3), and these levels are further decreased upon coexpression with the ZF-PHD3 fusion protein (lane 4). In a separate experiment, we transfected HEK293FT cells as described above but then stabilized HIF-1α with the proteasome inhibitor MG132 instead of hypoxia. In these circumstances, coexpression of PHD3 increased hydroxylation at Pro-564 of HIF-1α (Fig. 3E, lanes 2 and 3), and hydroxylation was further increased upon coexpression of the ZF-PHD3 fusion (lane 4). These experiments provide evidence that the zinc finger domain is sufficient to enhance the capacity of PHD3 to hydroxylate and destabilize HIF-1α.

Loss of zinc finger integrity *in vivo* leads to increased *Epo* expression and erythrocytosis. To evaluate our model *in vivo*, we created a mouse line with an *Egln1* (*Phd2*) knock-in allele containing the C36S/C42S mutation (here referred to as ZF) (Fig. 4A to D). As shown previously (Fig. 1C), this mutation abolishes association with the PXLE motif. Crosses between *Egln1*$^{ZF/+}$ mice yielded the expected genotypes, but *Egln1*$^{ZF/ZF}$ mice were born at a sub-Mendelian frequency (12% instead of the predicted 25%; 670 pups were genotyped). Similar to findings with *Egln1*$^{-/-}$ embryos (11), we noted that embryonic lethality appeared to occur at embryonic day 12.5 (E12.5) (Table 1), as no dead embryos were observed from litters at E11.5 and *Egln1*$^{ZF/ZF}$ embryos were observed at close to a Mendelian ratio at this age.

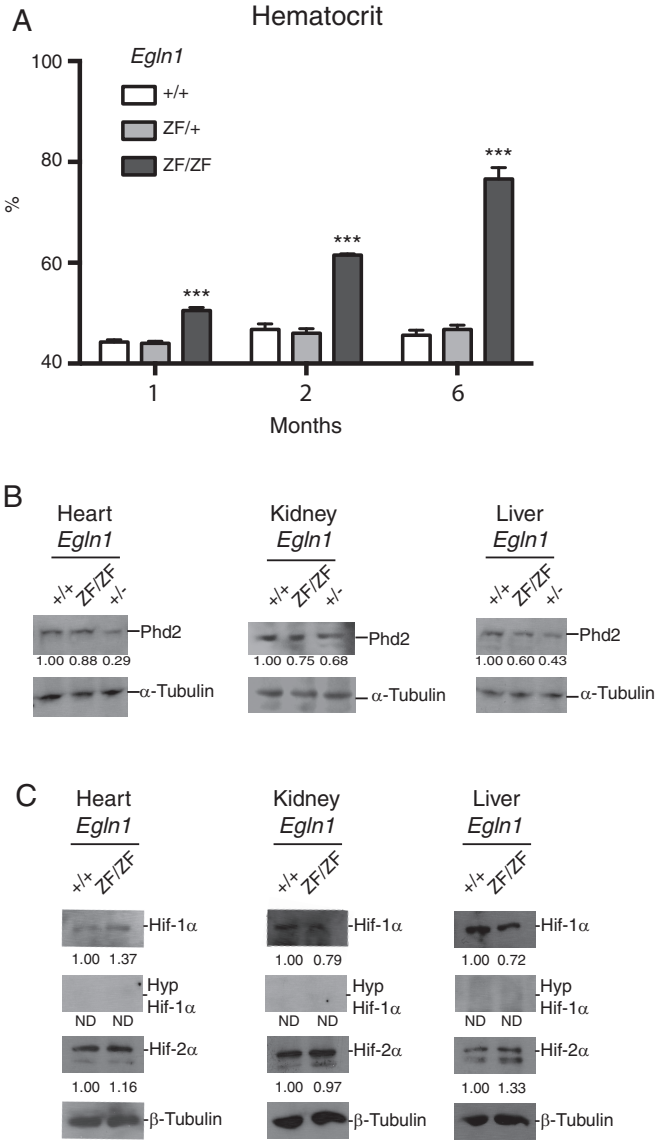

FIG 8 (A) Homozygous (*Egln1*$^{ZF/ZF}$) knock-in mice showed significantly increased hematocrit over time, whereas heterozygous (*Egln1*$^{ZF/+}$) knock-in mice showed no difference from *Egln1*$^{+/+}$ mice at any time point tested. The error bars represent SEM; $n = 4$ per group. ***, $P < 0.001$. (B) Western blots for assessing Phd2 and α-tubulin protein levels in heart, kidney, and liver tissues from 3-month-old *Egln1*$^{+/+}$, *Egln1*$^{ZF/ZF}$, and *Egln1*$^{+/-}$ mice. (C) Western blots for assessing Hif-1α, hydroxylated Hif-1α (HypHif-1), and Hif-2α protein levels in heart, kidney, and liver tissues from 3-month-old *Egln1*$^{+/+}$ and *Egln1*$^{ZF/ZF}$ mice. The numbers below the bands indicate relative intensities by densitometry compared to the WT and corrected for tubulin intensity. ND, not detectable.

Previous studies suggested that developmental defects in placenta formation are responsible for the embryonic-lethal phenotype in *Egln1*-null mice (11). Real-time PCR analysis of Hif target genes from *Egln1*$^{+/+}$ and *Egln1*$^{ZF/ZF}$ E11.5 placentas showed increases in the latter for the Hif targets *Vegfa* and *Egln3* (Fig. 5A and B). *Pgk1* transcripts were increased as well, though the increase did

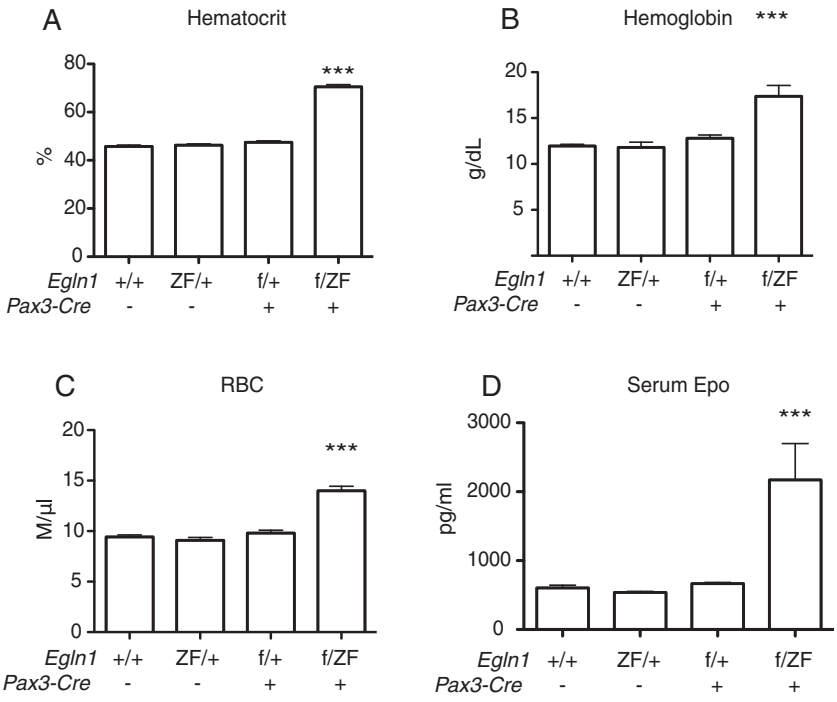

FIG 9 Two-month-old *Pax3*-Cre; *Egln1*$^{f/ZF}$ mice show increases in hematocrit (A), hemoglobin (B), red blood cell count (C), and serum Epo (D). The error bars represent SEM; $n = 3$ to 5 per group. ***, $P < 0.001$ by Student's t test.

not reach statistical significance. These observations offer evidence that Phd2 function is impaired at this stage of placental development. The prior studies also reported changes in gene expression related to placental development in *Egln1*$^{-/-}$ placentas, including an increase in *Ascl2* (*Mash2*) and decreases in *Gcm1* and *Tfeb* expression (11). We examined these genes and found that mRNA levels trended toward changes in the same direction (Fig. 5D to F) as in the previous report. However, they did not reach statistical significance; the incomplete penetrance of the embryonic-lethal phenotype in *Egln1*$^{ZF/ZF}$ compared to *Egln1*$^{-/-}$ embryos might account for this difference.

We noted a plethoric (ruddy) appearance in *Egln1*$^{ZF/ZF}$ mice (Fig. 6A) and observed elevated hematocrits (78% versus 49%), hemoglobin levels (22.2 versus 13.5 g/dl), red blood cell counts, serum Epo levels, and renal *Epo* mRNA levels compared to *Egln1*$^{+/+}$ controls (Fig. 6B to F). Of note, we saw no statistically significant changes in either white blood cell counts (+/+, $6.67 \times 10^3 \pm 3.01 \times 10^3$/μl, versus ZF/ZF, $6.20 \times 10^3 \pm 2.42 \times 10^3$/μl) or platelet counts (+/+, $458.44 \times 10^3 \pm 163.91 \times 10^3$/μl, versus ZF/ZF, $468.00 \times 10^3 \pm 102.68 \times 10^3$/μl). Hepatic *Epo* expression is normally very low in adult mice, and we found that hepatic *Epo* mRNA levels were low in comparison to those from kidneys and were not increased in *Egln1*$^{ZF/ZF}$ mice (Fig. 6G). We conclude from these studies that the kidney is the likely source of circulating Epo in these mice. Upon examination of several Hif target genes in a number of tissues, we found that most showed no evidence of significant alteration in *Egln1*$^{ZF/ZF}$ mice (Fig. 7). A modest mRNA increase was observed for *Slc2a1* (*Glut1*), encoding a glucose transporter regulated transcriptionally by Hif, in the kidneys of *Egln1*$^{ZF/ZF}$ mice, though similar changes were not seen in the hearts of these animals (Fig. 7C). The erythrocytosis in *Egln1*$^{ZF/ZF}$ mice was age dependent, more severe at 6 months than at 1 month of age (Fig. 8A). In contrast, heterozygous *Egln1*$^{ZF/+}$ mice did not display erythrocytosis at any time point (Fig. 8A). Taken together, these findings provide *in vivo* evidence that mutation of the Phd2 zinc finger leads to a loss-of-function allele. Western blots of tissue extracts from *Egln1*$^{ZF/ZF}$ mice revealed levels of Phd2 that were intermediate between those of *Egln1*$^{+/+}$ and *Egln1*$^{+/-}$ mice (Fig. 8B). *Egln1*$^{+/-}$ mice displayed, at most, very mild erythrocytosis (HCT, Egln1$^{+/+}$, ~48%, versus Egln1$^{+/-}$, ~53%) (16, 29); hence, the markedly increased erythrocytosis observed in *Egln1*$^{ZF/ZF}$ mice (HCT, 78%) cannot be accounted for by changes in Phd2 protein abundance. The levels of Hif-α in these tissues appeared to be either unchanged or, at best, only modestly altered (Fig. 8C); for example, in heart and liver, we observed modest increases in Hif-1α and Hif-2α, respectively. These results were not wholly unexpected, because in many tissues, Phd1 and Phd3 display functional redundancy with Phd2. For example, loss of all three Phd isoforms is necessary for hepatic induction of Epo expression in the adult mouse (35). Western blotting for hydroxylated proline 564 (Hyp-564) in Hif-1α was negative; as a control, the antibody did react with lysate from Hif-1α cDNA-transfected, MG132-treated cells (Fig. 3E and data not shown). This suggests that hydroxylated Hif-1α subunits are rapidly degraded by Vhl *in vivo*, preempting their detection.

To further examine whether the *Egln1*^{ZF} allele is a gain- or loss-of-function allele, we crossed *Egln1*$^{ZF/+}$ with *Egln1*$^{+/-}$ mice. These crosses, however, failed to yield *Egln1*$^{ZF/-}$ compound heterozygotes (37 pups were genotyped). As mentioned above, constitutive global loss of *Egln1* leads to placental defects and is embryonic lethal (11). The failure to generate these heterozygotes suggests that a single *Egln1*^{ZF} allele is insufficient to rescue the *Egln1*$^{-/-}$ phenotype, consistent with the *Egln1*^{ZF} allele being a hypomorphic allele. This notion

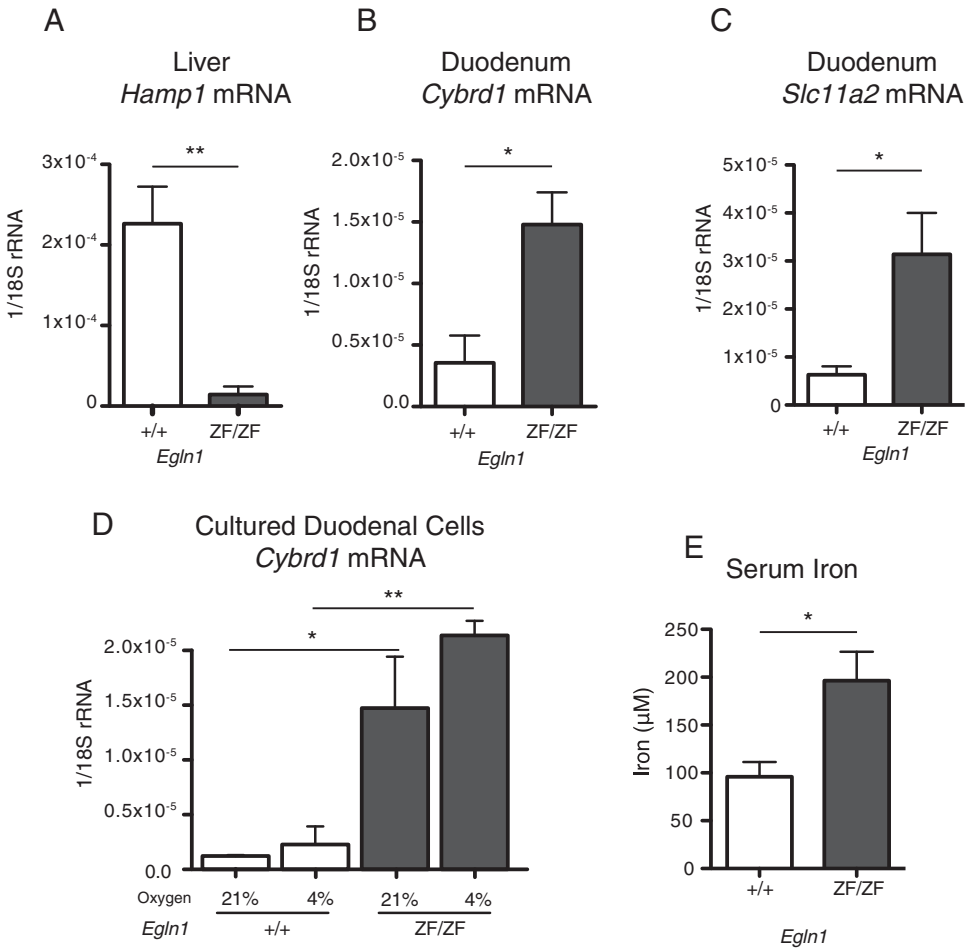

FIG 10 *Egln1*$^{ZF/ZF}$ mice display increased iron mobilization. (A) Real-time PCR analysis of hepatic *Hamp1* mRNA levels. (B and C) Real-time PCR analysis of duodenal enterocyte scrapings showing significant increases in *Cybrd1* (*DcytB*) (B) and *Slc11a2* (*Dmt1*) (C) mRNA levels in *Egln1*$^{ZF/ZF}$ mice relative to *Egln1*$^{+/+}$ controls. (D) Real-time PCR analysis of *Cybrd1* expression from *in vitro*-cultured duodenal enterocytes. (E) Serum iron is increased in *Egln1*$^{ZF/ZF}$ mice relative to *Egln1*$^{+/+}$ controls. (A to C and E) $n = 5$ per group; (D) $n = 4$ per group. The error bars represent SEM. *, $P < 0.05$; **, $P < 0.01$ by Student's *t* test.

is also consistent with the observation of sub-Mendelian frequency of *Egln1*$^{ZF/ZF}$ mice obtained from *Egln1*$^{ZF/+}$ crosses.

In additional experiments, we crossed *Egln1*$^{ZF/+}$ mice with mice harboring a heterozygous conditional knockout of *Egln1* in the Epo-producing cells of the kidney (*Pax3*-Cre; *Egln1*$^{f/+}$) (16). We observed that *Pax3*-Cre; *Egln1*$^{f/ZF}$ mice, like the *Egln1*$^{ZF/ZF}$ mice, displayed markedly increased hematocrit (69.87% ± 1.91% versus 48.38% ± 1.95%; $P < 0.001$), hemoglobin (17.37 ± 1.19 g/dl versus 11.80 ± 0.58 g/dl; $P < 0.001$), red blood cell counts ($13.99 \times 10^6 \pm 0.46 \times 10^6$/μl versus $9.088 \times 10^6 \pm 0.28 \times 10^6$/μl; $P < 0.001$), and serum Epo levels (2,172 ± 526 pg/ml versus 539 ± 14.73 pg/ml; $P < 0.001$) relative to *Egln1*$^{ZF/+}$ mice (Fig. 9). These data provide additional evidence that, within the Epo-producing cells of the kidney, *Egln1*^{ZF} is a loss-of-function allele.

The *Egln1*^{ZF} allele leads to increased iron transport gene expression and iron mobilization. Erythropoiesis is tightly coupled with iron mobilization (36). Iron mobilization, in turn, is critically regulated by, and inversely correlated with, hepdicin (Hamp1) levels. We found a 15-fold reduction in liver *Hamp1* mRNA transcript levels in *Egln1*$^{ZF/ZF}$ mice relative to *Egln1*$^{+/+}$ littermate controls (Fig. 10A). Decreased *Hamp1* mRNA is likely secondary to the Epo-induced erythrocytosis, potentially mediated by erythropoiesis-associated expression of erythroferrone (37, 38). Furthermore, we observed increased duodenal expression of the Hif-2α target genes, *Cybrd1* (*Dcytb*) and *Slc11a2* (*Dmt1*), which play important roles in the transport of iron across the duodenal epithelium (Fig. 10B and C) (39, 40). To determine if these changes were due to a cell-autonomous response *in vivo*, *Egln1*$^{+/+}$ and *Egln1*$^{ZF/ZF}$ duodenal epithelial cells were cultured *in vitro* and examined for expression of *Cybrd1* under both normoxia and mild hypoxia (4% O_2) (41) to simulate conditions present in the duodenum *in vivo*. *Cybrd1* expression in *Egln1*$^{ZF/ZF}$ duodenal cells remained high under both conditions, suggesting that it is a cell-autonomous response to reduced Phd2 activity (Fig. 10D). *Slc11a2* expression, in contrast, was unchanged between *Egln1*$^{+/+}$ and *Egln1*$^{ZF/ZF}$ cells under the same conditions (data not shown); however, the interpretation of this result is complicated by the low level of *Slc11a2* expression in *Egln1*$^{+/+}$ primary cell culture compared to duodenal scrapings. That being said, it remains possible that the increases observed *in vivo* are, at least in part, due to a cell-extrinsic mechanism distinct from *Slc11a2* regulation by Hif. Measurements of serum iron levels in *Egln1*$^{ZF/ZF}$ mice were increased nearly 2-fold relative to WT mice (Fig. 10E). This change, consistent with Phd2 loss of function and the changes in mRNA expression profiles described

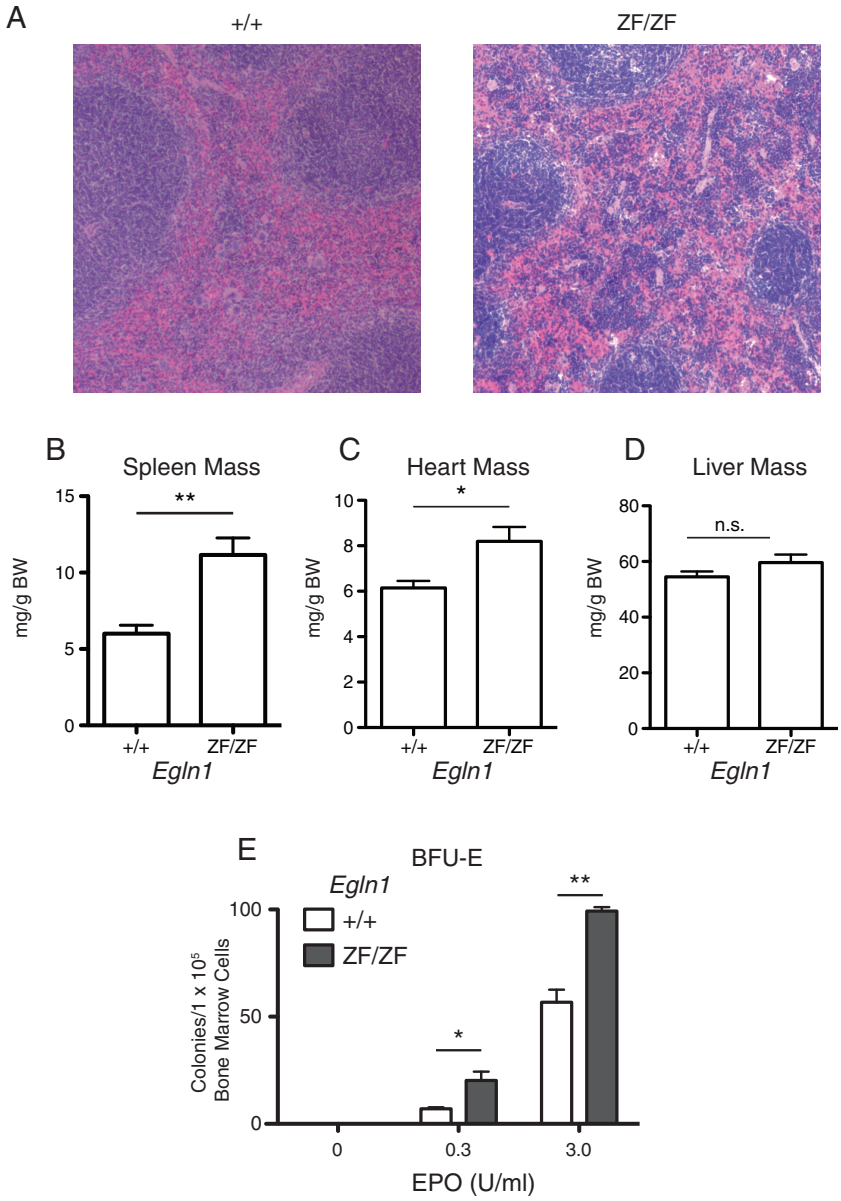

FIG 11 *Egln1*$^{ZF/ZF}$ mice display splenic erythropoiesis and increased BFU-E proliferation. (A) Hematoxylin- and eosin-stained sections of spleen from *Egln1*$^{+/+}$ mice and *Egln1*$^{ZF/ZF}$ mice. The latter shows splenic erythropoiesis. (B and C) Spleen mass (B) and heart mass (C) (relative to individual body weight) in 6-month-old *Egln1*$^{ZF/ZF}$ mice were significantly increased compared to *Egln1*$^{+/+}$ mice. $n = 5$ per group. (D) Liver mass was unchanged compared to *Egln1*$^{+/+}$ mice. $n = 5$ per group. (E) BFU-E colony formation assays were performed on bone marrow cells from *Egln1*$^{+/+}$ and *Egln1*$^{ZF/ZF}$ mice. After 9 days of culture, the latter displayed increased colony formation at both low and high levels of EPO. $n = 5$ per group. (B to E) The error bars represent SEM. *, $P < 0.05$; **, $P < 0.01$ by Student's *t* test.

above, occurred despite greatly increased red blood cell mass, which contains the largest pool of iron in the body.

The *Egln1*^{ZF} allele is associated with splenic erythropoiesis, increased BFU-E proliferation, and changes in pulmonary function. The spleens of *Egln1*$^{ZF/ZF}$ mice showed evidence of splenic erythropoiesis, and spleen mass was increased (Fig. 11A and B). Heart mass was also increased slightly, possibly a result of increased red blood cell mass, while other organs, such as the liver, were unaffected (Fig. 11C and D). In light of prior work (16, 29) and to address the possibility that *Egln1*$^{ZF/ZF}$ mice have features of primary erythrocytosis, we examined the proliferation of bone marrow cells in response to increasing levels of EPO by BFU-E assay. We found, indeed, that larger numbers of BFU-E were observed from the bone marrow of *Egln1*$^{ZF/ZF}$ than from *Egln1*$^{+/+}$ mice at two different EPO concentrations (Fig. 11E). Whether this is due entirely to preexisting expansion of the BFU-E within the bone marrow of *Egln1*$^{ZF/ZF}$ mice or whether there might be a contribution of hypersensitivity of BFU-E to EPO will require further investigation. To further evaluate these animals, we examined the role that Phd2 plays in respiration. Prior work had indicated that loss of Phd2 catalytic activity could lead to increased respiration (15, 16). We found that *Egln1*$^{ZF/ZF}$ mice displayed increased ven-

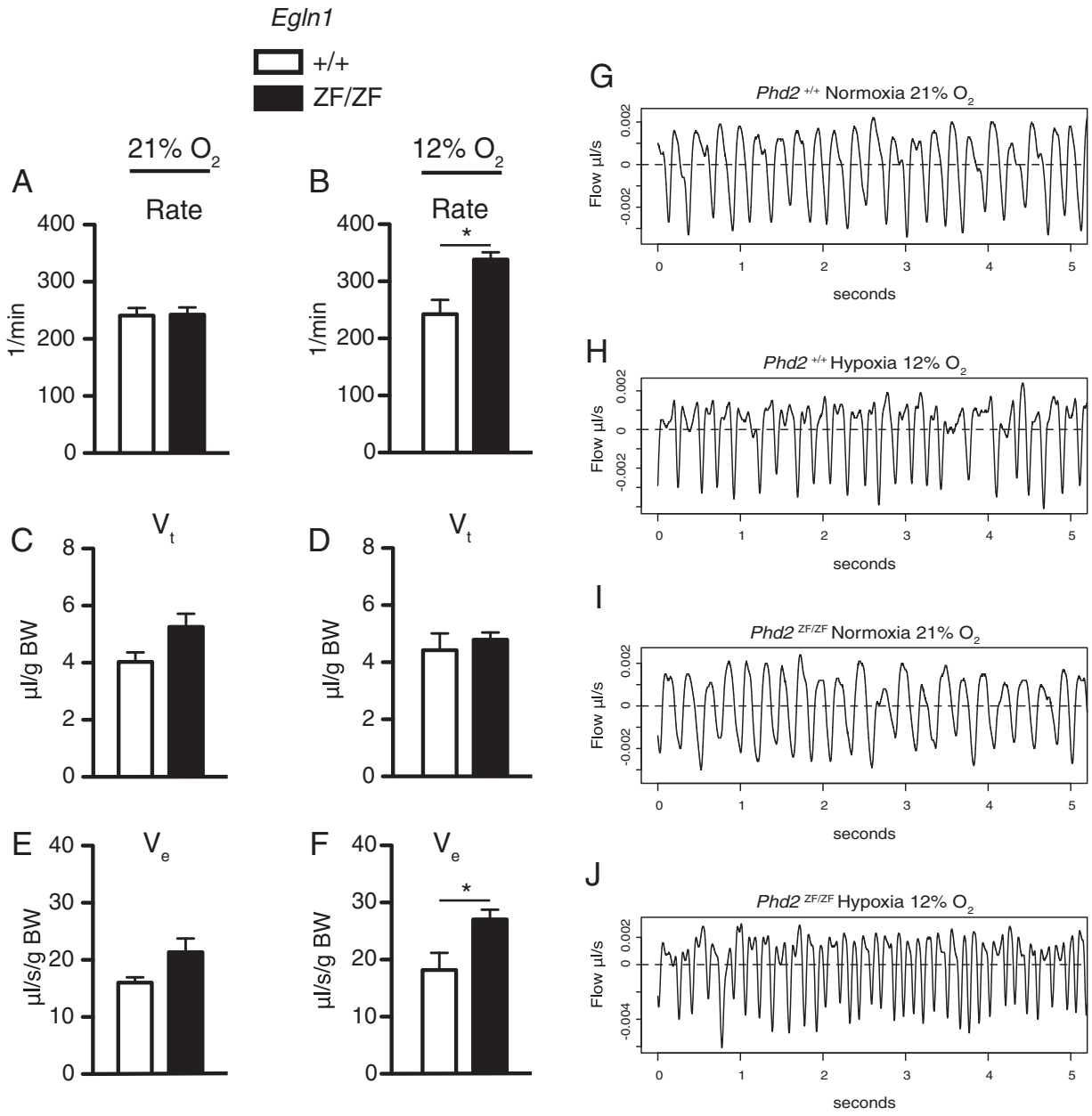

FIG 12 *Egln1*$^{ZF/ZF}$ mice display increased respiratory frequency and minute ventilation sensitivity to hypoxic challenge. (A to F) Respiration rate (A and B), tidal volume (C and D), and minute ventilation (E and F) obtained by whole-body plethysmography under normoxia (A, C, and E) and hypoxia (B, D, and F). The error bars represent SEM; $n = 5$ per group for all experiments. *, $P < 0.05$ by Student's t test. (G to I) Representative plethysmography traces from *Egln1*$^{+/+}$ (G and H) and *Egln1*$^{ZF/ZF}$ (I and J) mice showing increased frequency of respiration of the latter compared to the former under hypoxia (H and J); traces under normoxia (G and I) are also shown. The mice were 1 month of age.

tilatory frequency under hypoxic stress (12% oxygen), leading to increased minute ventilation (Fig. 12A to J), consistent with *Egln1* loss of function. Hence, *Egln1*$^{ZF/ZF}$ mice displayed evidence of an enhanced hypoxic ventilatory response (HVR). From these and the other studies presented here, we conclude that the *Egln1*^{ZF} allele is a loss-of-function allele.

DISCUSSION

The function of the zinc finger of PHD2 has been elusive and the subject of numerous studies (22, 23, 42–44). A fundamental question is whether it serves a positive or negative regulatory role. Our *in vitro* studies indicated that the zinc finger of PHD2 can facilitate the interaction of a heterologous protein (BirA) with HIF-α, consistent with our proposal that the zinc finger recruits PHD2 to the HSP90 pathway (Fig. 2). Furthermore, this interaction displays some degree of specificity for HSP90/HIF-α complexes, as the interaction with an alternate bHLH-PAS domain-containing transcription factor and HSP90 client, AHR, appeared to be weaker (Fig. 3B). Compellingly, the knock-in mouse described here, in which the zinc finger had been ablated, displayed upregulation of erythropoiesis, increased proliferation of erythroid precursors, increased iron mobilization, and an increased hypoxic

ventilatory response, all findings consistent with its being a loss-of-function allele. Indeed, similar observations have been reported in studies of humans and mice with genetic alterations resulting in augmented HIF signaling (45–51). Altogether, these findings demonstrate a critical positive regulatory role for the zinc finger of PHD2.

Our studies point to the kidney being the likely source of circulating Epo in *Egln1*$^{ZF/ZF}$ mice (Fig. 6F). In the Epo-producing cells of the kidney, Phd2 plays a critical role in the control of Hif-2α and subsequent Epo production (16, 52), which cannot be compensated for by either Phd1 or Phd3. In the present study, an important role for the Phd2 zinc finger in the renal Epo-producing cells is highlighted by the observation that coupling the *Egln1*^{ZF} allele with the *Pax3-Cre*; *Egln1*^{f} allele that conditionally deletes *Egln1* in these cells yielded a dramatic erythrocytosis that was not observed with either of the alleles alone (Fig. 9A to D). The situation in the kidney may be contrasted with that in the liver, in which *Egln1* loss alone was insufficient to induce *Epo* transcription (35). Indeed, we did not observe any significant increase in hepatic *Epo* mRNA levels in *Egln1*$^{ZF/ZF}$ mice (Fig. 6G).

While homozygous knockout of *Egln1* leads to embryonic lethality in the mouse (11), mice with two copies of the *Egln1*^{ZF} allele are viable. Though they appeared at a lower frequency than expected, the *Egln1*$^{ZF/ZF}$ mice unequivocally demonstrated that the integrity of the zinc finger is not essential for viability in the mouse. Interestingly, the zinc finger of the PHD2 homologue in *Caenorhabditis elegans*, Egl-9, is similarly not essential for viability (53). Moreover, that study showed that it is not even essential for inhibition of Hif-1 activity in the organism (53). This is in contrast to the present study, which demonstrates a critical role for the zinc finger in mice, at least in the regulation of genes such as *Epo*.

High-altitude-adapted Tibetans harbor a PHD2 variant (D4E/C127S) (54, 55) that, as with the murine Phd2 mutant studied here, is defective in its interaction with p23 (23). The present data, therefore, suggest that Tibetan PHD2 is likely to be a loss-of-function allele that in turn may be a critical component of their remarkable adaptation to chronic hypoxia (56). It must be noted, though, that the Tibetan D4E/C127S allele and the C36S/C42S allele reported here are unlikely to be identical. For example, Tibetan PHD2, unlike the Phd2 mutant studied here, maintains interaction with other proteins of the HSP90 pathway that contain PXLE motifs, including FKBP38 and HSP90 itself (23). Hence, additional studies will be required to more completely define the nature of the Tibetan *EGLN1* allele, as well as how it interacts with variants at other genetic loci, such as the *EPAS1* (*HIF2A*) gene, that show evidence of natural selection in this population (57–63).

ACKNOWLEDGMENTS

We thank Tobias Raabe of the University of Pennsylvania Perelman School of Medicine Gene Targeting facility for performing the ES cell electroporations and Jean Richa of the University of Pennsylvania Perelman School of Medicine Transgenic Core Facility for conducting injections of targeted ES cells into blastocysts.

HHS (National Institutes of Health [NIH]) provided funding to Frank S. Lee under grants R01-CA153347, R21-HL120751, and R01-DK567611. The University of Pennsylvania Research Foundation provided funding to Frank S. Lee. HHS (NIH) provided funding to Patrick R. Arsenault under grant number T32-DK007780. The Perelman School of Medicine Transgenic Core Facility is supported by the Institute for Diabetes, Obesity, and Cardiovascular Metabolism (grant DK019525), the Center for Molecular Studies in Digestive and Liver Diseases (grant DK050306), and the Abramson Cancer Center (grant CA016520).

We declare that we have no conflicts of interest.

FUNDING INFORMATION

This work, including the efforts of Frank S. Lee, was funded by HHS | National Institutes of Health (NIH) (R01-CA153347, R21-HL120751, and R01-DK567611). This work, including the efforts of Patrick R. Arsenault, was funded by HHS | National Institutes of Health (NIH) (T32-DK007780).

REFERENCES

1. **Semenza GL.** 2012. Hypoxia-inducible factors in physiology and medicine. Cell **148:**399–408. http://dx.doi.org/10.1016/j.cell.2012.01.021.
2. **Kaelin WG, Jr, Ratcliffe PJ.** 2008. Oxygen sensing by metazoans: the central role of the HIF hydroxylase pathway. Mol Cell **30:**393–402. http://dx.doi.org/10.1016/j.molcel.2008.04.009.
3. **Majmundar AJ, Wong WJ, Simon MC.** 2010. Hypoxia-inducible factors and the response to hypoxic stress. Mol Cell **40:**294–309. http://dx.doi.org/10.1016/j.molcel.2010.09.022.
4. **Ivan M, Kondo K, Yang H, Kim W, Valiando J, Ohh M, Salic A, Asara JM, Lane WS, Kaelin WG, Jr.** 2001. HIFα targeted for VHL-mediated destruction by proline hydroxylation: implications for O2 sensing. Science **292:**464–468. http://dx.doi.org/10.1126/science.1059817.
5. **Jaakkola P, Mole DR, Tian YM, Wilson MI, Gielbert J, Gaskell SJ, Kriegsheim AA, Hebestreit HF, Mukherji M, Schofield CJ, Maxwell PH, Pugh CW, Ratcliffe PJ.** 2001. Targeting of HIF-α to the von Hippel-Lindau ubiquitylation complex by O_2-regulated prolyl hydroxylation. Science **292:**468–472. http://dx.doi.org/10.1126/science.1059796.
6. **Yu F, White SB, Zhao Q, Lee FS.** 2001. HIF-1α binding to VHL is regulated by stimulus-sensitive proline hydroxylation. Proc Natl Acad Sci U S A **98:**9630–9635. http://dx.doi.org/10.1073/pnas.181341498.
7. **Lendahl U, Lee KL, Yang H, Poellinger L.** 2009. Generating specificity and diversity in the transcriptional response to hypoxia. Nat Rev Genet **10:**821–832. http://dx.doi.org/10.1038/nrg2665.
8. **Wenger RH, Stiehl DP, Camenisch G.** 2005. Integration of oxygen signaling at the consensus HRE. Sci STKE **2005:**re12.
9. **Epstein AC, Gleadle JM, McNeill LA, Hewitson KS, O'Rourke J, Mole DR, Mukherji M, Metzen E, Wilson MI, Dhanda A, Tian YM, Masson N, Hamilton DL, Jaakkola P, Barstead R, Hodgkin J, Maxwell PH, Pugh CW, Schofield CJ, Ratcliffe PJ.** 2001. C. elegans EGL-9 and mammalian homologs define a family of dioxygenases that regulate HIF by prolyl hydroxylation. Cell **107:**43–54. http://dx.doi.org/10.1016/S0092-8674(01)00507-4.
10. **Bruick RK, McKnight SL.** 2001. A conserved family of prolyl-4-hydroxylases that modify HIF. Science **294:**1337–1340. http://dx.doi.org/10.1126/science.1066373.
11. **Takeda K, Ho VC, Takeda H, Duan LJ, Nagy A, Fong GH.** 2006. Placental but not heart defects are associated with elevated hypoxia-inducible factor α levels in mice lacking prolyl hydroxylase domain protein 2. Mol Cell Biol **26:**8336–8346. http://dx.doi.org/10.1128/MCB.00425-06.
12. **Lee FS, Percy MJ.** 2011. The HIF pathway and erythrocytosis. Annu Rev Pathol **6:**165–192. http://dx.doi.org/10.1146/annurev-pathol-011110-130321.
13. **Takeda K, Aguila HL, Parikh NS, Li X, Lamothe K, Duan LJ, Takeda H, Lee FS, Fong GH.** 2008. Regulation of adult erythropoiesis by prolyl hydroxylase domain proteins. Blood **111:**3229–3235. http://dx.doi.org/10.1182/blood-2007-09-114561.
14. **Minamishima YA, Moslehi J, Bardeesy N, Cullen D, Bronson RT, Kaelin WG, Jr.** 2008. Somatic inactivation of the PHD2 prolyl hydroxylase causes polycythemia and congestive heart failure. Blood **111:**3236–3244. http://dx.doi.org/10.1182/blood-2007-10-117812.
15. **Bishop T, Talbot NP, Turner PJ, Nicholls LG, Pascual A, Hodson EJ, Douglas G, Fielding JW, Smith TG, Demetriades M, Schofield CJ, Robbins PA, Pugh CW, Buckler KJ, Ratcliffe PJ.** 2013. Carotid body hyperplasia and enhanced ventilatory responses to hypoxia in mice with heterozygous deficiency of PHD2. J Physiol **591:**3565–3577. http://dx.doi.org/10.1113/jphysiol.2012.247254.

16. **Arsenault PR, Pei F, Lee R, Kerestes H, Percy MJ, Keith B, Simon MC, Lappin TR, Khurana TS, Lee FS.** 2013. A knock-in mouse model of human PHD2 gene-associated erythrocytosis establishes a haploinsufficiency mechanism. J Biol Chem **288:**33571–33584. http://dx.doi.org/10.1074/jbc.M113.482364.
17. **Loenarz C, Coleman ML, Boleininger A, Schierwater B, Holland PW, Ratcliffe PJ, Schofield CJ.** 2011. The hypoxia-inducible transcription factor pathway regulates oxygen sensing in the simplest animal, *Trichoplax adhaerens*. EMBO Rep **12:**63–70. http://dx.doi.org/10.1038/embor.2010.170.
18. **Taylor MS.** 2001. Characterization and comparative analysis of the EGLN gene family. Gene **275:**125–132. http://dx.doi.org/10.1016/S0378-1119(01)00633-3.
19. **Rytkonen KT, Williams TA, Renshaw GM, Primmer CR, Nikinmaa M.** 2011. Molecular evolution of the metazoan PHD-HIF oxygen-sensing system. Mol Biol Evol **28:**1913–1926. http://dx.doi.org/10.1093/molbev/msr012.
20. **Matthews JM, Bhati M, Lehtomaki E, Mansfield RE, Cubeddu L, Mackay JP.** 2009. It takes two to tango: the structure and function of LIM, RING, PHD and MYND domains. Curr Pharm Des **15:**3681–3696. http://dx.doi.org/10.2174/138161209789271861.
21. **Liu Y, Chen W, Gaudet J, Cheney MD, Roudaia L, Cierpicki T, Klet RC, Hartman K, Laue TM, Speck NA, Bushweller JH.** 2007. Structural basis for recognition of SMRT/N-CoR by the MYND domain and its contribution to AML1/ETO's activity. Cancer Cell **11:**483–497. http://dx.doi.org/10.1016/j.ccr.2007.04.010.
22. **Song D, Li LS, Heaton-Johnson KJ, Arsenault PR, Master SR, Lee FS.** 2013. Prolyl hydroxylase domain protein 2 (PHD2) binds a Pro-Xaa-Leu-Glu motif, linking it to the heat shock protein 90 pathway. J Biol Chem **288:**9662–9674. http://dx.doi.org/10.1074/jbc.M112.440552.
23. **Song D, Li LS, Arsenault PR, Tan Q, Bigham AW, Heaton-Johnson KJ, Master SR, Lee FS.** 2014. Defective Tibetan PHD2 binding to p23 links high altitude adaptation to altered oxygen sensing. J Biol Chem **289:**14656–14665. http://dx.doi.org/10.1074/jbc.M113.541227.
24. **Copeland NG, Jenkins NA, Court DL.** 2001. Recombineering: a powerful new tool for mouse functional genomics. Nat Rev Genet **2:**769–779.
25. **Liu P, Jenkins NA, Copeland NG.** 2003. A highly efficient recombineering-based method for generating conditional knockout mutations. Genome Res **13:**476–484. http://dx.doi.org/10.1101/gr.749203.
26. **Yagi T, Ikawa Y, Yoshida K, Shigetani Y, Takeda N, Mabuchi I, Yamamoto T, Aizawa S.** 1990. Homologous recombination at c-fyn locus of mouse embryonic stem cells with use of diphtheria toxin A-fragment gene in negative selection. Proc Natl Acad Sci U S A **87:**9918–9922. http://dx.doi.org/10.1073/pnas.87.24.9918.
27. **Laird PW, Zijderveld A, Linders K, Rudnicki MA, Jaenisch R, Berns A.** 1991. Simplified mammalian DNA isolation procedure. Nucleic Acids Res **19:**4293. http://dx.doi.org/10.1093/nar/19.15.4293.
28. **Nik AM, Carlsson P.** 2013. Separation of intact intestinal epithelium from mesenchyme. Biotechniques **55:**42–44. http://dx.doi.org/10.2144/000114055.
29. **Li X, Sutherland S, Takeda K, Fong GH, Lee FS.** 2010. Integrity of the prolyl hydroxylase domain protein 2:erythropoietin pathway in aging mice. Blood Cells Mol Dis **45:**9–19. http://dx.doi.org/10.1016/j.bcmd.2010.03.003.
30. **Schneider CA, Rasband WS, Eliceiri KW.** 2012. NIH Image to ImageJ: 25 years of image analysis. Nat Methods **9:**671–675. http://dx.doi.org/10.1038/nmeth.2089.
31. **Drorbaugh JE, Fenn WO.** 1955. A barometric method for measuring ventilation in newborn infants. Pediatrics **16:**81–87.
32. **Pettersen EF, Goddard TD, Huang CC, Couch GS, Greenblatt DM, Meng EC, Ferrin TE.** 2004. UCSF Chimera—a visualization system for exploratory research and analysis. J Comput Chem **25:**1605–1612. http://dx.doi.org/10.1002/jcc.20084.
33. **London N, Raveh B, Cohen E, Fathi G, Schueler-Furman O.** 2011. Rosetta FlexPepDock Web server—high resolution modeling of peptide-protein interactions. Nucleic Acids Res **39:**W249–W253. http://dx.doi.org/10.1093/nar/gkr431.
34. **Wochnik GM, Ruegg J, Abel GA, Schmidt U, Holsboer F, Rein T.** 2005. FK506-binding proteins 51 and 52 differentially regulate dynein interaction and nuclear translocation of the glucocorticoid receptor in mammalian cells. J Biol Chem **280:**4609–4616. http://dx.doi.org/10.1074/jbc.M407498200.
35. **Minamishima YA, Kaelin WG, Jr.** 2010. Reactivation of hepatic EPO synthesis in mice after PHD loss. Science **329:**407. http://dx.doi.org/10.1126/science.1192811.
36. **Ganz T.** 2013. Systemic iron homeostasis. Physiol Rev **93:**1721–1741. http://dx.doi.org/10.1152/physrev.00008.2013.
37. **Kautz L, Jung G, Valore EV, Rivella S, Nemeth E, Ganz T.** 2014. Identification of erythroferrone as an erythroid regulator of iron metabolism. Nat Genet **46:**678–684. http://dx.doi.org/10.1038/ng.2996.
38. **Liu Q, Davidoff O, Niss K, Haase VH.** 2012. Hypoxia-inducible factor regulates hepcidin via erythropoietin-induced erythropoiesis. J Clin Invest **122:**4635–4644. http://dx.doi.org/10.1172/JCI63924.
39. **Mastrogiannaki M, Matak P, Keith B, Simon MC, Vaulont S, Peyssonnaux C.** 2009. HIF-2α, but not HIF-1α, promotes iron absorption in mice. J Clin Invest **119:**1159–1166. http://dx.doi.org/10.1172/JCI38499.
40. **Shah YM, Matsubara T, Ito S, Yim SH, Gonzalez FJ.** 2009. Intestinal hypoxia-inducible transcription factors are essential for iron absorption following iron deficiency. Cell Metab **9:**152–164. http://dx.doi.org/10.1016/j.cmet.2008.12.012.
41. **He G, Shankar RA, Chzhan M, Samouilov A, Kuppusamy P, Zweier JL.** 1999. Noninvasive measurement of anatomic structure and intraluminal oxygenation in the gastrointestinal tract of living mice with spatial and spectral EPR imaging. Proc Natl Acad Sci U S A **96:**4586–4591. http://dx.doi.org/10.1073/pnas.96.8.4586.
42. **Choi KO, Lee T, Lee N, Kim JH, Yang EG, Yoon JM, Kim JH, Lee TG, Park H.** 2005. Inhibition of the catalytic activity of hypoxia-inducible factor-1α-prolyl-hydroxylase 2 by a MYND-type zinc finger. Mol Pharmacol **68:**1803–1809.
43. **Barth S, Nesper J, Hasgall PA, Wirthner R, Nytko KJ, Edlich F, Katschinski DM, Stiehl DP, Wenger RH, Camenisch G.** 2007. The peptidyl prolyl cis/trans isomerase FKBP38 determines hypoxia-inducible transcription factor prolyl-4-hydroxylase PHD2 protein stability. Mol Cell Biol **27:**3758–3768. http://dx.doi.org/10.1128/MCB.01324-06.
44. **Barth S, Edlich F, Berchner-Pfannschmidt U, Gneuss S, Jahreis G, Hasgall PA, Fandrey J, Wenger RH, Camenisch G.** 2009. Hypoxia-inducible factor prolyl-4-hydroxylase PHD2 protein abundance depends on integral membrane anchoring of FKBP38. J Biol Chem **284:**23046–23058. http://dx.doi.org/10.1074/jbc.M109.032631.
45. **Ang SO, Chen H, Hirota K, Gordeuk VR, Jelinek J, Guan Y, Liu E, Sergueeva AI, Miasnikova GY, Mole D, Maxwell PH, Stockton DW, Semenza GL, Prchal JT.** 2002. Disruption of oxygen homeostasis underlies congenital Chuvash polycythemia. Nat Genet **32:**614–621. http://dx.doi.org/10.1038/ng1019.
46. **Haase VH, Glickman JN, Socolovsky M, Jaenisch R.** 2001. Vascular tumors in livers with targeted inactivation of the von Hippel-Lindau tumor suppressor. Proc Natl Acad Sci U S A **98:**1583–1588. http://dx.doi.org/10.1073/pnas.98.4.1583.
47. **Hickey MM, Lam JC, Bezman NA, Rathmell WK, Simon MC.** 2007. von Hippel-Lindau mutation in mice recapitulates Chuvash polycythemia via hypoxia-inducible factor-2α signaling and splenic erythropoiesis. J Clin Invest **117:**3879–3889.
48. **Percy MJ, Zhao Q, Flores A, Harrison C, Lappin TR, Maxwell PH, McMullin MF, Lee FS.** 2006. A family with erythrocytosis establishes a role for prolyl hydroxylase domain protein 2 in oxygen homeostasis. Proc Natl Acad Sci U S A **103:**654–659. http://dx.doi.org/10.1073/pnas.0508423103.
49. **Percy MJ, Furlow PW, Lucas GS, Li X, Lappin TR, McMullin MF, Lee FS.** 2008. A gain-of-function mutation in the *HIF2A* gene in familial erythrocytosis. N Engl J Med **358:**162–168. http://dx.doi.org/10.1056/NEJMoa073123.
50. **Smith TG, Brooks JT, Balanos GM, Lappin TR, Layton DM, Leedham DL, Liu C, Maxwell PH, McMullin MF, McNamara CJ, Percy MJ, Pugh CW, Ratcliffe PJ, Talbot NP, Treacy M, Robbins PA.** 2006. Mutation of von Hippel-Lindau tumour suppressor and human cardiopulmonary physiology. PLoS Med **3:**e290. http://dx.doi.org/10.1371/journal.pmed.0030290.
51. **Tan Q, Kerestes H, Percy MJ, Pietrofesa R, Chen L, Khurana TS, Christofidou-Solomidou M, Lappin TR, Lee FS.** 2013. Erythrocytosis and pulmonary hypertension in a mouse model of human *HIF2A* gain of function mutation. J Biol Chem **288:**17134–17144. http://dx.doi.org/10.1074/jbc.M112.444059.
52. **Franke K, Kalucka J, Mamlouk S, Singh RP, Muschter A, Weidemann A, Iyengar V, Jahn S, Wieczorek K, Geiger K, Muders M, Sykes AM, Poitz DM, Ripich T, Otto T, Bergmann S, Breier G, Baretton G, Fong GH, Greaves DR, Bornstein S, Chavakis T, Fandrey J, Gassmann M,**

Wielockx B. 2013. HIF-1α is a protective factor in conditional PHD2-deficient mice suffering from severe HIF-2α-induced excessive erythropoiesis. Blood **121:**1436–1445. http://dx.doi.org/10.1182/blood-2012-08-449181.

53. **Shao Z, Zhang Y, Powell-Coffman JA.** 2009. Two distinct roles for EGL-9 in the regulation of HIF-1-mediated gene expression in Caenorhabditis elegans. Genetics **183:**821–829. http://dx.doi.org/10.1534/genetics.109.107284.
54. **Lorenzo FR, Huff C, Myllymaki M, Olenchock B, Swierczek S, Tashi T, Gordeuk V, Wuren T, Ri-Li G, McClain DA, Khan TM, Koul PA, Guchhait P, Salama ME, Xing J, Semenza GL, Liberzon E, Wilson A, Simonson TS, Jorde LB, Kaelin WG, Jr, Koivunen P, Prchal JT.** 2014. A genetic mechanism for Tibetan high-altitude adaptation. Nat Genet **46:**951–956. http://dx.doi.org/10.1038/ng.3067.
55. **Xiang K, Ouzhuluobu Peng Y, Yang Z, Zhang X, Cui C, Zhang H, Li M, Zhang Y, Bianba, Gonggalanzi, Basang, Ciwangsangbu, Wu T, Chen H, Shi H, Qi X, Su B.** 2013. Identification of a Tibetan-specific mutation in the hypoxic gene EGLN1 and its contribution to high-altitude adaptation. Mol Biol Evol **30:**1889–1898. http://dx.doi.org/10.1093/molbev/mst090.
56. **Bigham AW, Lee FS.** 2014. Human high-altitude adaptation: forward genetics meets the HIF pathway. Genes Dev **28:**2189–2204. http://dx.doi.org/10.1101/gad.250167.114.
57. **Beall CM, Cavalleri GL, Deng L, Elston RC, Gao Y, Knight J, Li C, Li JC, Liang Y, McCormack M, Montgomery HE, Pan H, Robbins PA, Shianna KV, Tam SC, Tsering N, Veeramah KR, Wang W, Wangdui P, Weale ME, Xu Y, Xu Z, Yang L, Zaman MJ, Zeng C, Zhang L, Zhang X, Zhaxi P, Zheng YT.** 2010. Natural selection on EPAS1 (HIF2α) associated with low hemoglobin concentration in Tibetan highlanders. Proc Natl Acad Sci U S A **107:**11459–11464. http://dx.doi.org/10.1073/pnas.1002443107.
58. **Bigham A, Bauchet M, Pinto D, Mao X, Akey JM, Mei R, Scherer SW, Julian CG, Wilson MJ, Lopez Herraez D, Brutsaert T, Parra EJ, Moore LG, Shriver MD.** 2010. Identifying signatures of natural selection in Tibetan and Andean populations using dense genome scan data. PLoS Genet **6:**e1001116. http://dx.doi.org/10.1371/journal.pgen.1001116.
59. **Simonson TS, Yang Y, Huff CD, Yun H, Qin G, Witherspoon DJ, Bai Z, Lorenzo FR, Xing J, Jorde LB, Prchal JT, Ge R.** 2010. Genetic evidence for high-altitude adaptation in Tibet. Science **329:**72–75. http://dx.doi.org/10.1126/science.1189406.
60. **Yi X, Liang Y, Huerta-Sanchez E, Jin X, Cuo ZX, Pool JE, Xu X, Jiang H, Vinckenbosch N, Korneliussen TS, Zheng H, Liu T, He W, Li K, Luo R, Nie X, Wu H, Zhao M, Cao H, Zou J, Shan Y, Li S, Yang Q, Asan Ni P, Tian G, Xu J, Liu X, Jiang T, Wu R, Zhou G, Tang M, Qin J, Wang T, Feng S, Li G, Huasang, Luosang J, Wang W, Chen F, Wang Y, Zheng X, Li Z, Bianba Z, Yang G, Wang X, Tang S, Gao G, Chen Y, Luo Z, Gusang L, Cao Z, Zhang Q, Ouyang W, Ren X, Liang H, Zheng H, Huang Y, Li J, Bolund L, Kristiansen K, Li Y, Zhang Y, Zhang X, Li R, Li S, Yang H, Nielsen R, Wang J, Wang J.** 2010. Sequencing of 50 human exomes reveals adaptation to high altitude. Science **329:**75–78. http://dx.doi.org/10.1126/science.1190371.
61. **Peng Y, Yang Z, Zhang H, Cui C, Qi X, Luo X, Tao X, Wu T, Ouzhuluobu, Basang, Ciwangsangbu, Danzengduojie, Chen H, Shi H, Su B.** 2011. Genetic variations in Tibetan populations and high-altitude adaptation at the Himalayas. Mol Biol Evol **28:**1075–1081. http://dx.doi.org/10.1093/molbev/msq290.
62. **Wang B, Zhang YB, Zhang F, Lin H, Wang X, Wan N, Ye Z, Weng H, Zhang L, Li X, Yan J, Wang P, Wu T, Cheng L, Wang J, Wang DM, Ma X, Yu J.** 2011. On the origin of Tibetans and their genetic basis in adapting high-altitude environments. PLoS One **6:**e17002. http://dx.doi.org/10.1371/journal.pone.0017002.
63. **Xu S, Li S, Yang Y, Tan J, Lou H, Jin W, Yang L, Pan X, Wang J, Shen Y, Wu B, Wang H, Jin L.** 2011. A genome-wide search for signals of high-altitude adaptation in Tibetans. Mol Biol Evol **28:**1003–1011. http://dx.doi.org/10.1093/molbev/msq277.